

4. Results and Discussion

4.1 Introduction

This chapter provides the results from the incremental dynamic analysis (IDA) of the LA 9-story structure, which incorporates several different variations of fluid viscous damping. For each damping type, the structure was subjected to 12 different earthquakes, six near-field and six far-field, that were scaled to intensities that ranged from $S_a(T_1, 10\%)=0.1$ to 2.0 g, by 0.1 g increments. This means that the structure with each damping type was subjected to 240 earthquake time history analyses. The different types of fluid viscous dampers added to the structure include: linear dampers, $\alpha=1.0$, for 5, 10, 15, and 20% critical damping ratio, and nonlinear dampers, $\alpha=0.5$ and 1.5, calibrated for 1 and 5% drift at 10 and 20% critical damping ratio. Therefore, the structure was tested with eight different types of damping. The analysis also includes some tests with yielding damper braces. Originally it was assumed that the chevron damper braces would not be allowed to yield, but this assumption was reconsidered and some of the analysis was redone. The structure including yielding braces with $\alpha=0.5$ at 1% drift, $\alpha=1.0$, and $\alpha=1.5$ at 1% drift was subjected to five of the ground motions at intensities that range from 0.1-0.5g by 0.1g increments and 0.5-1.9 by 0.2g increments.

In this chapter, the results of the analysis are primarily discussed with IDA curves. The IDA curves are used to summarize structural behavior for a variable range of conditions, including earthquake type and intensity.

4.2 Critical Damping Ratio

The effect of critical damping ratio on peak base shear and peak interstory drift ratio (IDR) was investigated for the LA 9-story structure with linear fluid viscous dampers. The linear fluid viscous damping, which was added to the structure, was varied to four different levels of critical damping: 5, 10, 15, and 20%. IDA curves were created for

each earthquake at every level of damping. The changes in system behavior caused by the changes in damping are clearly identified in these curves.

The trend in structural response for different levels of damping was similar when subjecting the model to the different earthquakes. An example of structural behavior for different levels of critical damping when subjected to an LA ground motion can be seen in Figure 4.1 (a-b). These figures are the IDA plot when the structure is subjected to the LA11 earthquake.

The overall structural behavior displayed in Figure 4.1 (a) shows that as the critical damping ratio increases, the peak base shear increases. Figure 4.1 (b) indicates that as the level of critical damping increases, the interstory drift ratios (IDR) decreases. A more in-depth look at the base shear, presented in Figure 4.2, reveals that before the yield point the base shear decreases with increased critical damping. After the yield point, the curves for the different levels of damping flip and base shear increases with increased critical damping. From this observation, it can be concluded that fluid viscous damping behavior has different effects on a structure based on whether the structure performs in the elastic or inelastic range.

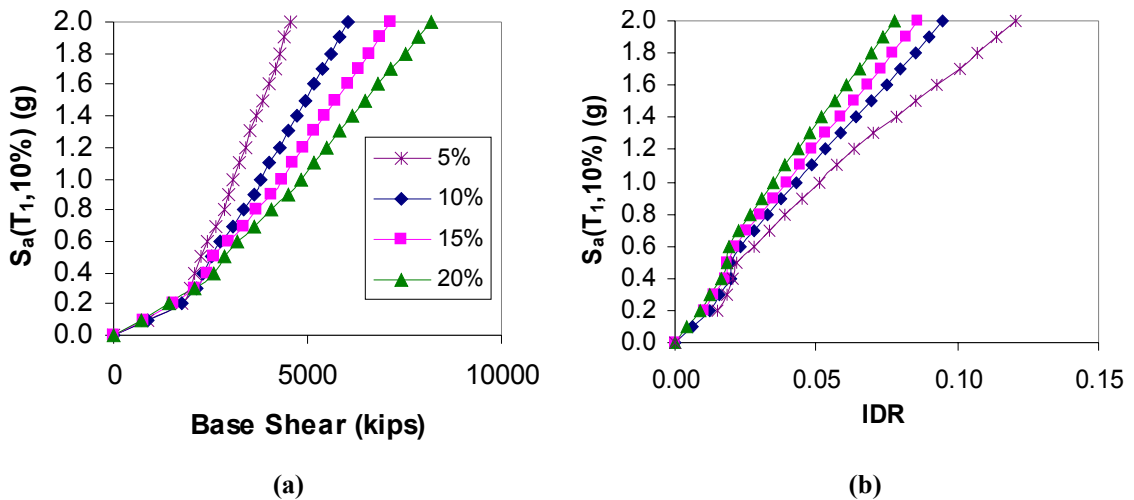


Figure 4.1: IDA Curves for $\alpha=1.0$, 5-20% Critical Damping, LA11

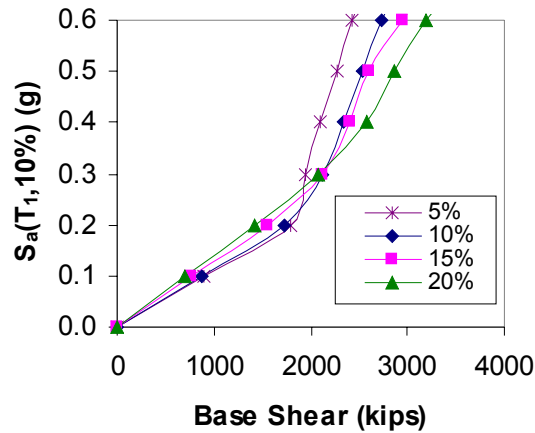


Figure 4.2: Close-up of IDA Curves for $\alpha=1.0$, 5-20% Critical Damping, LA11

The behavior exhibited in Figure 4.2 can be explained by examining the behavior of an elastic-perfectly-plastic, single degree of freedom (SDOF) system subjected to a sinusoidal loading function. The program *NONLIN* was used to analyze SDOF systems with 10%, 15%, and 20% critical damping ratios, subjected to sine waves with five different amplitudes. Figure 4.3 displays the plot of the total force for the 10%, 15%, and 20% damped structure subjected to a sine wave with the various amplitudes. Figure 4.4 (a-c) display plots of maximum spring force, damper force, and total force for the 10%, 15% and 20% damped structures subjected to sine waves with amplitudes of 7, 30, 60, 100, and 120 kips.

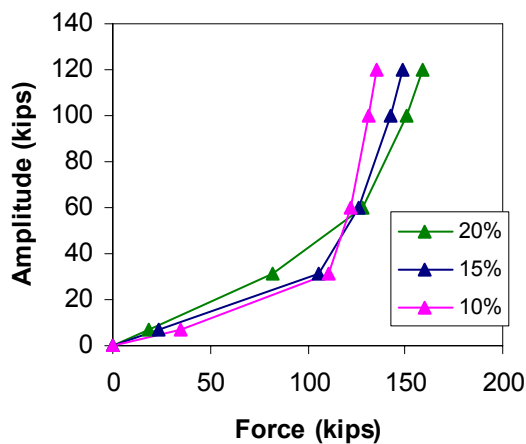


Figure 4.3: Total Force vs. Amplitude for 10, 15, and 20% Damped System

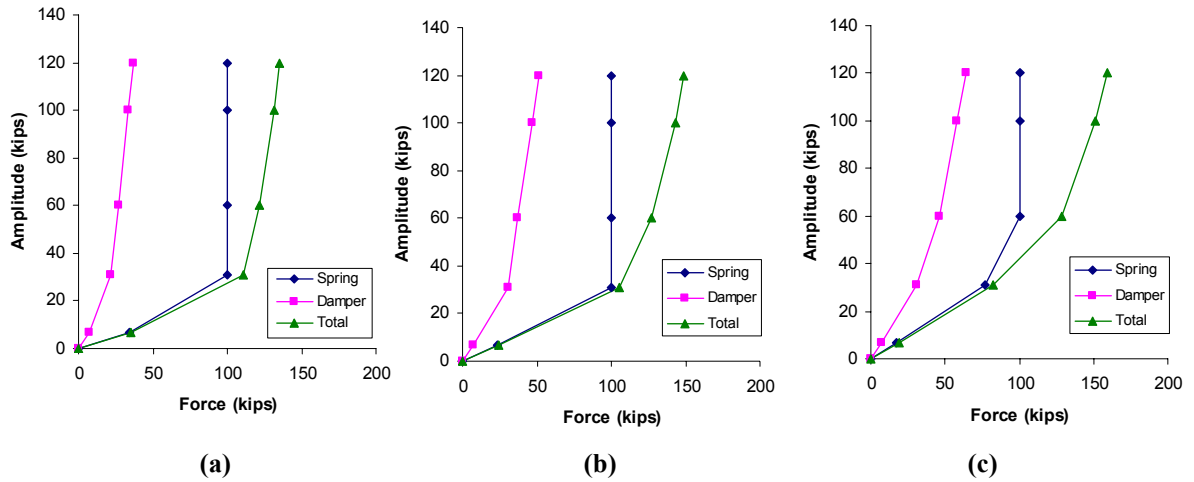
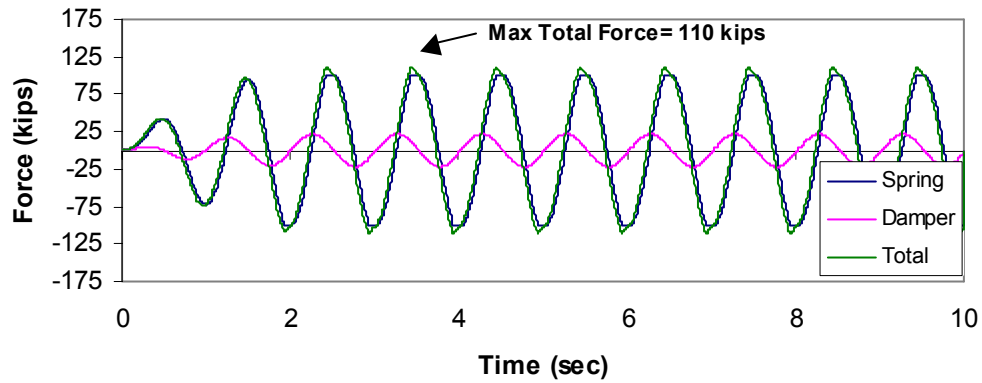
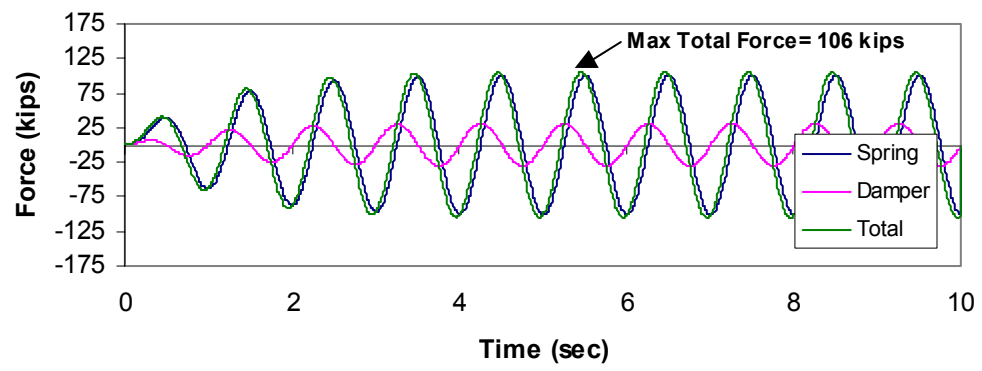


Figure 4.4 (a-c): Force vs. Amplitude for SDOF with (a) 10%, (b) 15%, and (c) 20% Damping Ratio

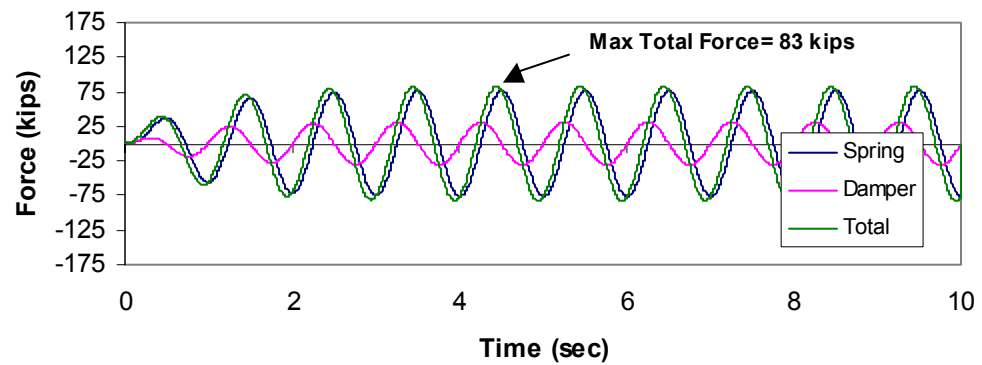
The first behavior to observe in Figure 4.3 is that, at the lower amplitudes, an increased damping ratio decreases total force, but at the higher amplitudes, where the system has yielded, increased damping ratio increases the total force. This behavior can be explained by Figure 4.4 (a-c), which demonstrates that at the higher amplitudes the maximum total force is close to being the full combination of the maximum spring force and the maximum damper force. Figure 4.4 (a-c) also displays, that at the lower amplitudes the maximum total force is much less than the combination of the maximum spring and damper forces. Finally, Figure 4.4 (a-c) illustrates that as damping ratio increases the spring force remains constant or decreases, while the damper force increases. These behaviors are explained in Figure 4.5 (a-c) and Figure 4.6 (a-c) which display time history plots of the forces for the SDOF system with different damping ratios at amplitudes where the system behaves elastically and where the system behaves inelastically.



(a)



(b)



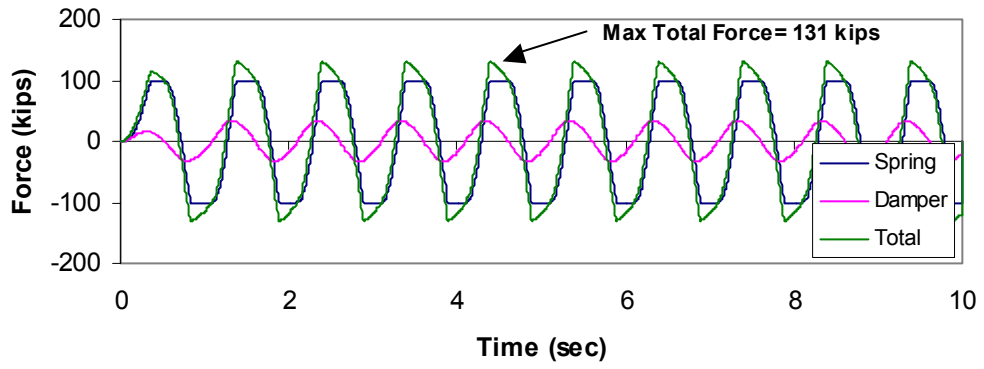
(c)

Figure 4.5 (a-c): Force T-H Plots for (a) 10%, (b) 15%, and (c) 20% Damped SDOF, Amp=30 in.

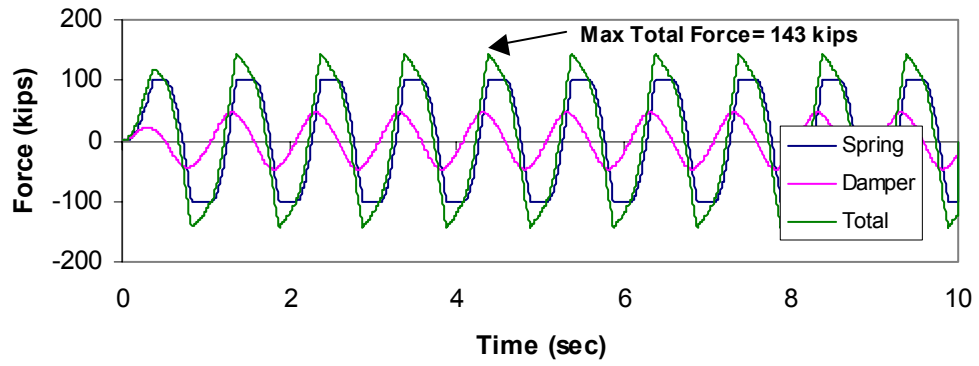
Figure 4.5 (a-c) is used to demonstrate the two different behaviors of the system when it behaves elastically. The first is that the spring force of the 10% damped systems is about 90° out-of-phase with the damper force. This means that when the spring force is at a maximum, the damper force equals zero, and vice versa. As the damping ratio increase

to 15% and 20% there is more of a phase lag and the total force is a larger combination of spring and damper forces, however the spring and damper forces are still almost out-of-phase. This explains why the total force in the elastic system is less than the full combination of maximum spring and damper forces. The other behavior exhibited by the elastic system in Figure 4.5 (a-b) is that as the damping ratio increases the maximum damper force stays the same, but the spring force decreases. This, in combination with the out-of-phase spring and damper forces is the reason that increased damping ratio decreases the total force in a structure that behaves elastically.

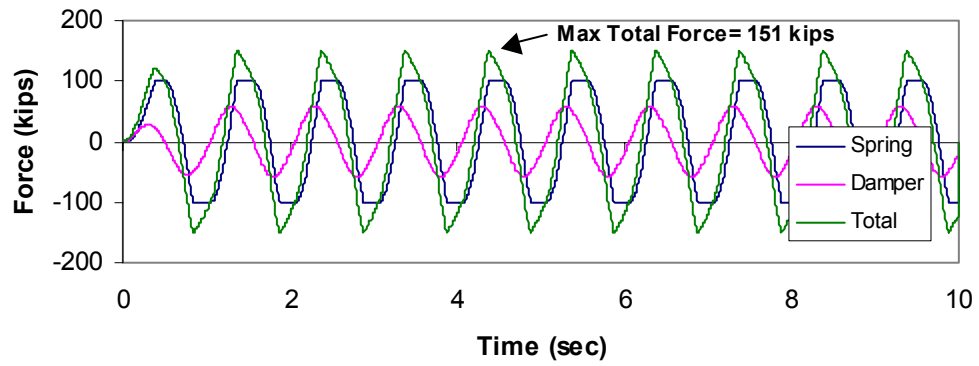
Figure 4.6 (a-b) is used to demonstrate three different behaviors of the system when it behaves inelastically. First, the system has yielded for all the levels of damping, and when the system yields it cannot develop a maximum spring force greater than the yield force. Therefore, as the damping ratio increases the maximum spring force remains the same. The second behavior is that as the damping ratio increases in the inelastic system the maximum damper forces also increase. Figure 4.6 (a-c) displays a maximum damper force of 33 kips for the 10% damped system, 47 kips for the 15% damped system, and 58 kips for the 20% damped system. The final behavior is that the slope of the spring force curve between peaks for the inelastic system is steeper than the slope of the spring force curve between the peaks for the elastic system. This results in a larger combination of spring and damper forces. Therefore, since the higher damping ratio in inelastic systems has an equal maximum spring force, a larger maximum damper force, and a combination of damper and spring forces which is more severe than in elastic systems, the total force will increase with increased damping ratio.



(a)



(b)



(c)

Figure 4.6 (a-c): Force T-H Plots for (a) 10%, (b) 15%, and (c) 20% Damped SDOF, Amp=100 in.

The point on an IDA plot at which the LA 9-story structure makes a transition in behavior for the different levels of critical damping has been defined as the yield point. In Figure 4.2, the yield point occurs at about $S_a(T_1, 10\%)=0.3g$. This represents the intensity at which structural members first undergo significant inelastic deformations. In the structure used for this study, the girders are the first elements to develop inelastic hinges. Figure 4.7 displays the location of each inelastic hinge that forms for the 20% critically damped structure subjected to the LA11 earthquake scaled to 0.3 g. As the earthquake intensity increases past 0.3 g, more inelastic hinges will form in the girders along with hinges at the base of the first-story columns, and eventually the panel zones will also yield. Yielding behavior at a higher intensity is illustrated in Figure 4.8, which displays the hinges formed when the 20% critically damped structure is subjected to the LA11 earthquake scaled to 0.7 g.

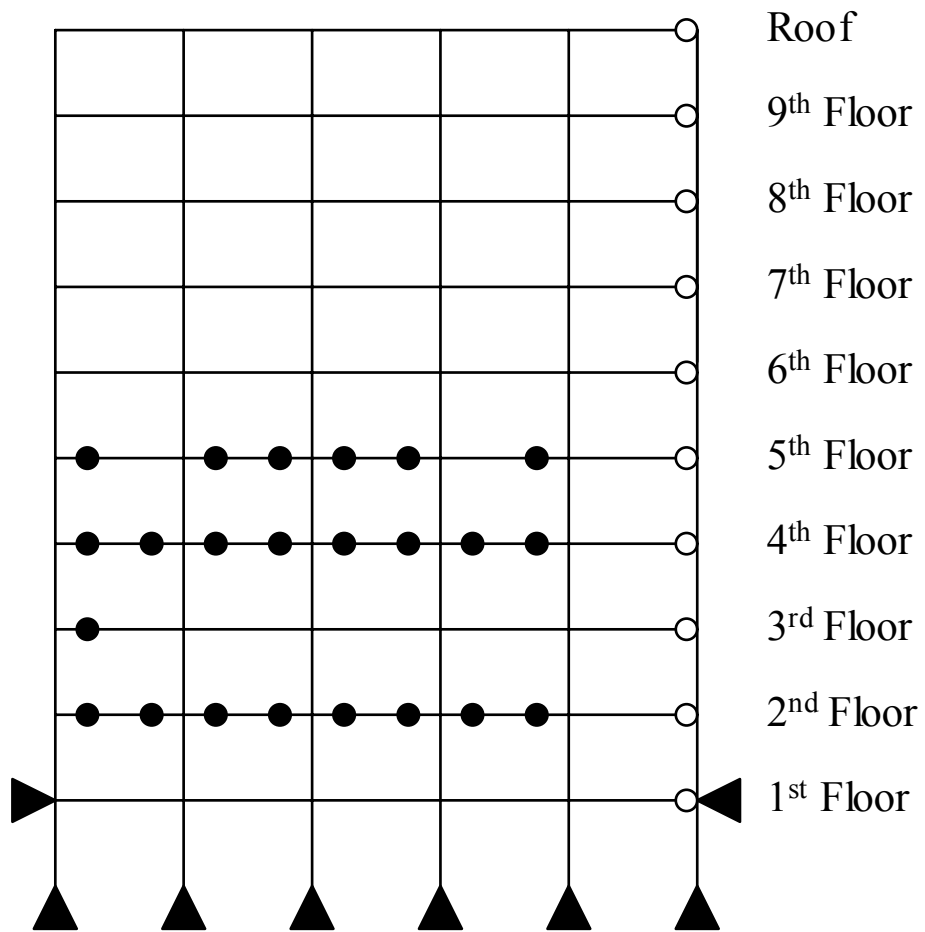


Figure 4.7: Inelastic Hinges for 20% Critically Damped Structure Subjected to LA11 at 0.3g

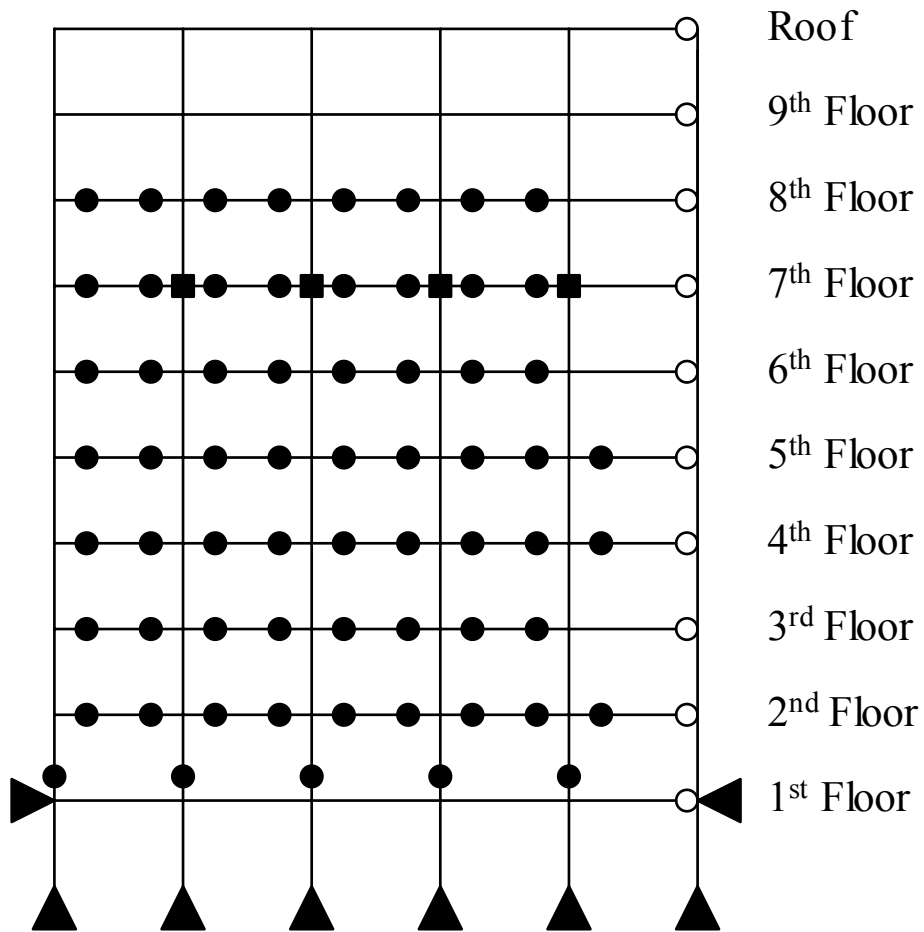


Figure 4.8 Inelastic Hinges for 20% Critically Damped Structure Subjected to LA11 at 0.7g

The reductions in IDR and the increases in base shear between 5% critical damping and the other levels of damping can be quantified in percent reduction IDA plots. These are plots of the percent reduction between 5% and the other levels of critical damping. The plots, shown in Figure 4.9 (a-b), give a better picture of the magnitude of the changes for different levels of ground motion intensity of the LA11 earthquake. Note that in the plots a negative decrease corresponds to an increase

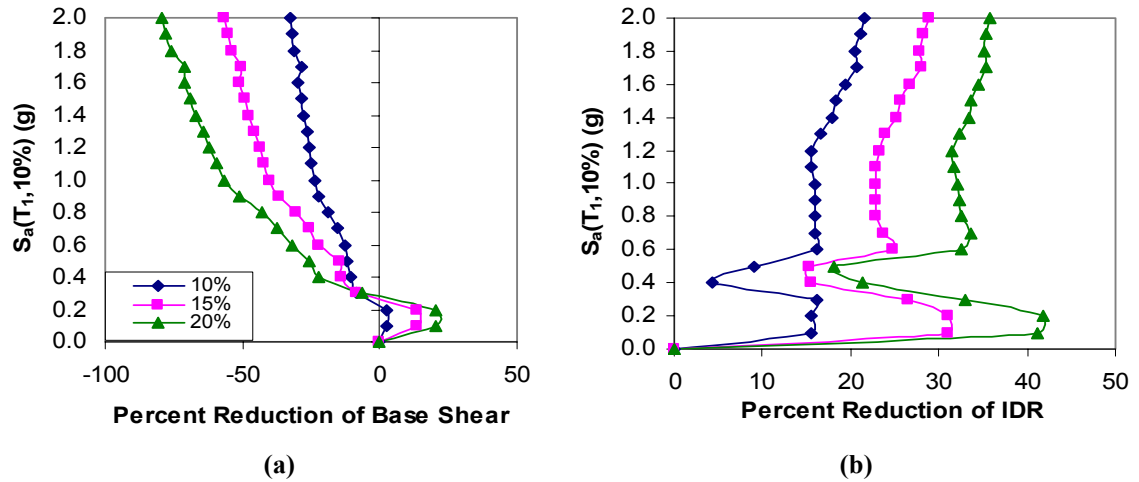


Figure 4.9 (a-b): Percent Reduction IDA Curves for $\alpha=1.0$, LA11

The behavior of the structure, when subjected to near-field ground motions, was expected to differ from the behavior shown previously when the structure was subjected to the LA ground motions. The reason for this difference is that the response to near-field earthquakes should be non-resonant and linear fluid viscous damping is, theoretically, only effective when the structure is vibrating near its resonant frequency.

An example of the actual behavior is displayed in Figure 4.10 (a-b), which plots the response of the LA 9-story structure subjected to the NF07 ground motion. The results in these plots are similar to the results found in Figure 4.10 (a-b). A more refined look at the base shear, illustrated in Figure 4.11, also shows that the behavior of the base shear in the structure is similar for the NF and LA earthquakes. These findings suggest that linear fluid viscous dampers are effective for reducing the response of structures subjected to near-field earthquakes.

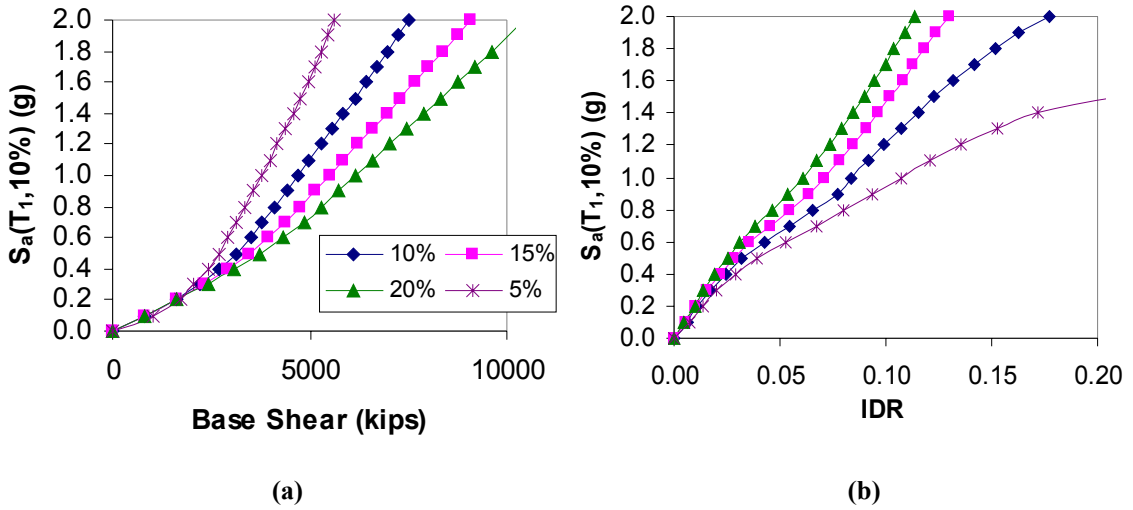


Figure 4.10 (a-b): IDA Curves for $\alpha=1.0$, 5-20% Critical Damping, NF07

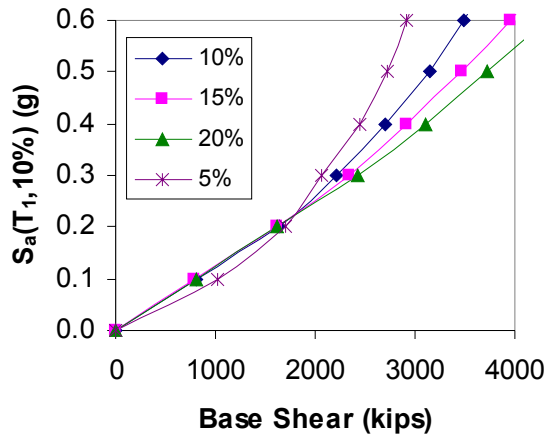


Figure 4.11: Close-up of IDA Curves for $\alpha=1.0$, 5-20% Critical Damping, NF07

Figure 4.12 (a-b) shows the percent reduction IDA curves for peak IDR and peak base shear. By comparing these reductions for NF07 to the reductions for LA11, it can be observed that the linear fluid viscous damping actually produces a greater reduction in IDR for the near-field earthquakes. Furthermore, the increase in base shear is about the same for the two different types of earthquakes. The IDA plots for the structure subjected to the other NF ground motions display behavior similar to that shown in the plots for NF07. This is significant because it contradicts a conclusion made by

researchers, such as Makris (1997), that viscous damping alone has little effect in reducing response to near-field motions.

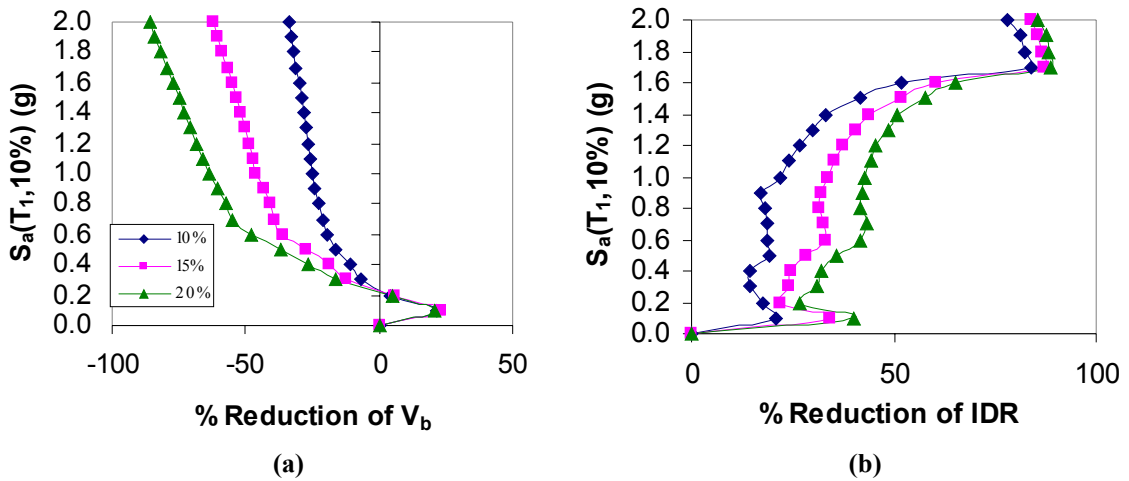


Figure 4.12 (a-b): Percent Reduction IDA Curves for $\alpha=1.0$, NF07

Appendix 2 presents the peak IDR and peak base shear IDA curves for each ground motion for each level of damping. Included in the appendix are close-ups of the peak base shear IDA curves and IDA plots of the percent reduction for peak base shear and peak IDR. The results in these plots are all similar to those previously displayed in Figure 4.1 through Figure 4.12. Therefore, the following points can summarize the behavior of the LA 9-story structure, with different levels of linear fluid viscous damping: as the level of critical damping increases, peak IDR decreases, peak base shear decreases prior to yield and increases after yield, and finally, linear fluid viscous damping is effective for both LA and NF ground motions.

4.3 Damping Exponent

In this study the damping exponent, α in Equation 2.8, was varied to investigate the effect of nonlinear dampers on dynamic structural response. Nonlinear dampers with $\alpha=0.5$ and 1.5 were selected so that the study would include two different types of nonlinear damping. When $\alpha=0.5$, the force-velocity curve of the damper exhibits a softening relationship, and when $\alpha=1.5$, the force-velocity curves does the opposite and

hardens. The nonlinear dampers were calibrated, using the method discussed in Section 3.2.5.2, for comparison with a 10% and 20% critical damping ratio and for 1% and 5% drift. The results, shown in this section, illustrate and compare the behavior of the structural system when the different types of nonlinear damping, calibrated for different levels of drift, are used. This section also compares the response of the structure with the nonlinear dampers to the response with linear dampers. Included in the IDA plots is the curve for the 5% linear critically damped structure. Essentially this curve represents a structure with 5% inherent damping and no supplemental dampers. The curve serves as a basis for comparison on each of the plots.

4.3.1 Peak Base Shear IDA Plots

The behavior of the structure, with respect to peak base shear, as the earthquake intensity increases past the yield point is similar for both the LA and NF ground motions and for a 10% and 20% critical damping ratio. Base shear slope is relatively uniform before yield and the slope increases to varying degrees after yield. The greatest increase in slope comes when $\alpha=0.5$ calibrated at 1% drift, and the least increase is produced by $\alpha=1.5$ calibrated at 1% drift. Examples of this behavior are illustrated in Figure 4.13 and Figure 4.14. These are the base shear IDA curves for the LA 9-story structure, with varying types of damping at 10% and 20% critical damping ratios, for the LA11 and NF07 earthquakes.

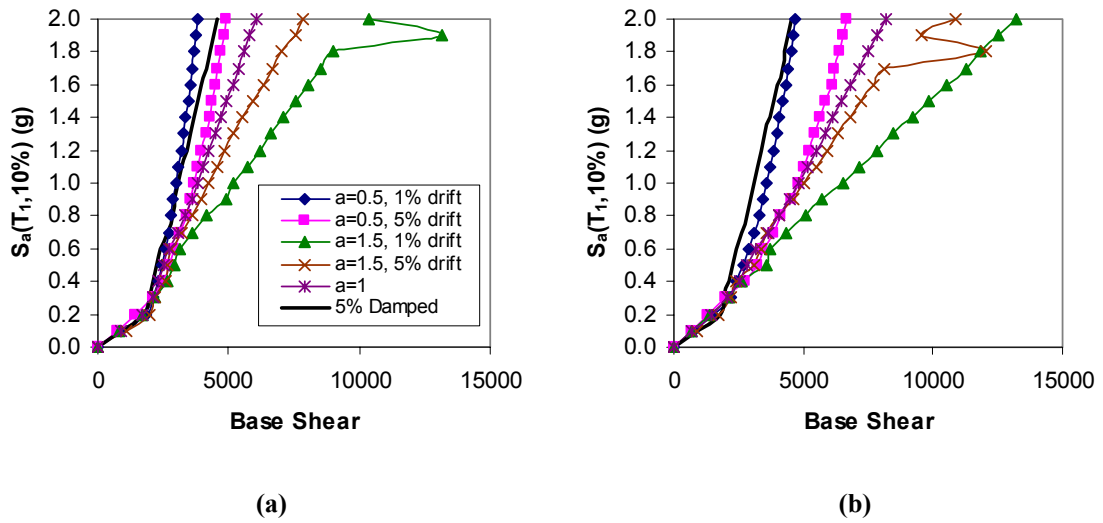


Figure 4.13 (a-b): Base Shear IDA Curves for LA11 Ground Motions with 10% (a) and 20% (b) Critical Damping Ratio

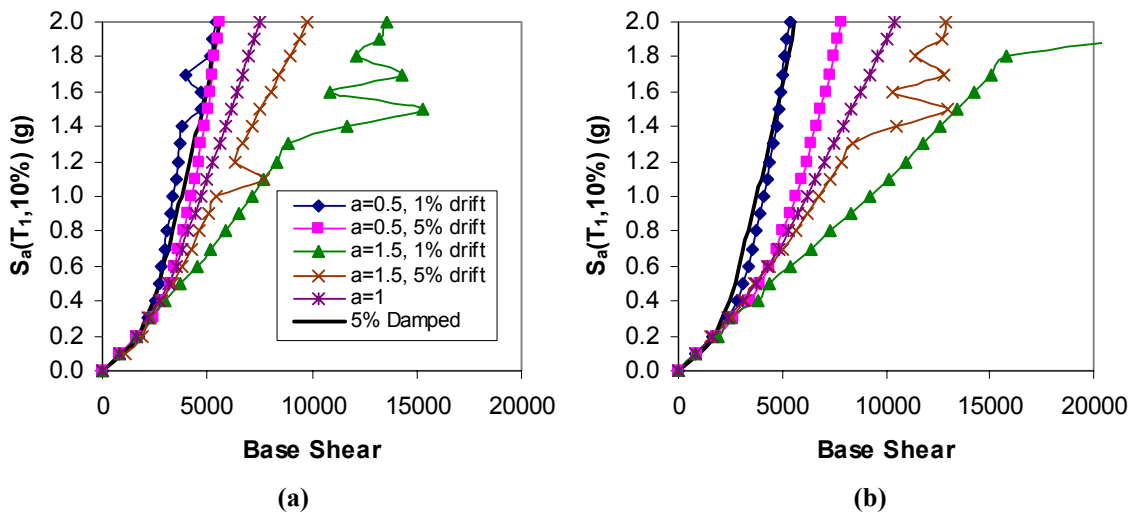


Figure 4.14 (a-b): Base Shear IDA Curves for NF07 Ground Motions with 10% (a) and 20% (b) Critical Damping Ratio

4.3.2 Peak Interstory Drift Ratio IDA Plots

The behavior of the peak IDR curves varies more than the peak base shear for the different earthquakes. However, generally the IDR curves for different damping types are less uniform than the peak base shear curves before the yield point. After yield the IDR curves tend to soften for $\alpha \leq 1$ and harden slightly, or maintain a constant slope, for $\alpha > 1$. The poorest response is primarily observed when $\alpha=0.5$, calibrated for 1% drift,

while the best response is when $\alpha=1.5$, calibrated for 1% drift. An interesting note is that when the structure has 10% critical damping the response with $\alpha=0.5$ at 1% is worse than the response for the 5% damped structure; however, at the same time the peak base shear is less. Figure 4.15 (a-b) and Figure 4.16 (a-b) illustrate this behavior in IDA plots for the LA 9-story structure, with varying types of damping at 10% and 20% critical damping ratios, for the LA11 and NF07 earthquakes.

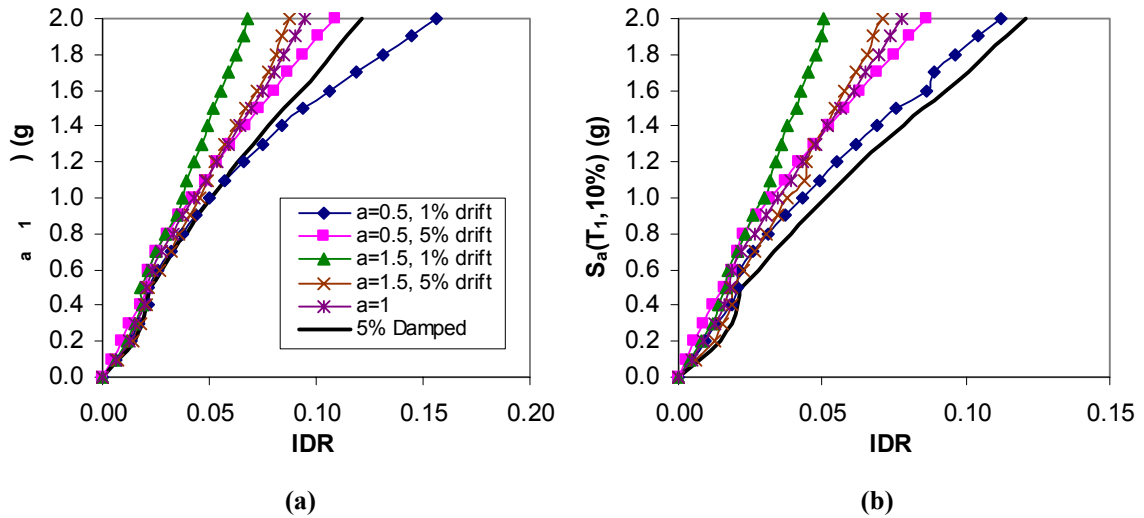


Figure 4.15 (a-b): Interstory Drift Ratio IDA Curves for LA11 Ground Motions with 10% (a) and 20% (b) Critical Damping Ratio

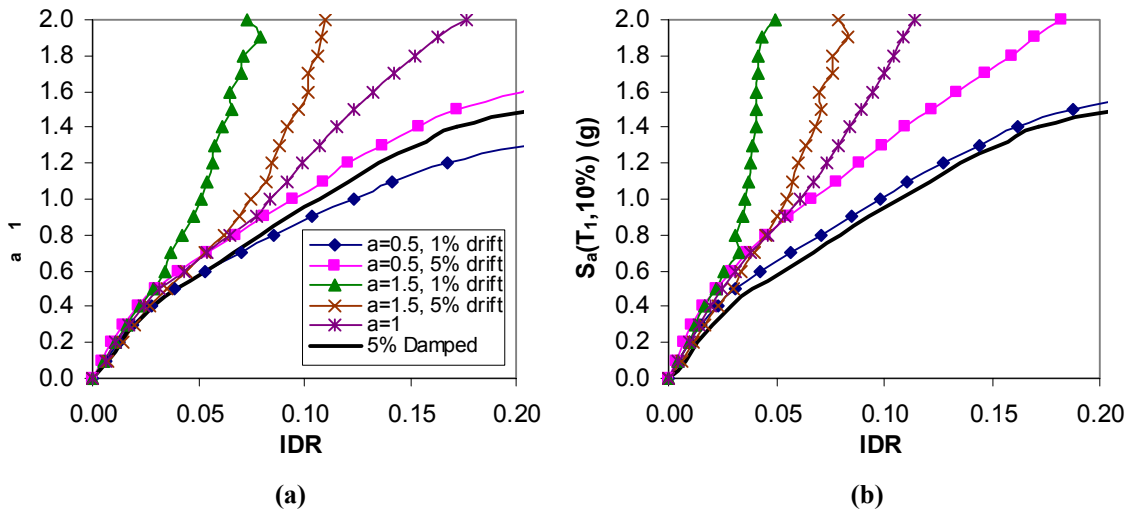


Figure 4.16 (a-b): Interstory Drift Ratio IDA Curves for NF07 Ground Motions with 10% (a) and 20% (b) Critical Damping Ratio

The behavior displayed in Figure 4.13-Figure 4.16 is intended to represent the behavior exhibited by the structure with different damping types for all of the earthquakes, both LA and NF. A comparison of the drift IDA curves for the LA and NF ground motions may lead to conclusions that there is more dispersion between the IDA curves of the different damping types when the structure is subjected to the NF ground motions. However, this only applies when comparing results for the two ground motions, LA11 and NF07. Appendix B displays that the dispersion between the IDA curves for the different damping types varies for all of the ground motions. In summary, the analyses have shown that structures incorporating dampers with a value of $\alpha > 1$ is best suited to reduce peak drift demands. However, an increasingly undesirable level of peak base shear is created in these systems with increased earthquake intensity. The opposite is true for $\alpha < 1$; these dampers are best suited to decrease peak base shear, but peak drift demands may increase to undesired levels.

4.3.3 Percent Reduction IDA Plots

The percent difference between the structure with the nonlinear dampers and the structure with linear dampers was plotted versus earthquake intensity. These plots provide a quantitative comparison of the nonlinear and linear dampers that may not be possible by just looking at the IDA plots presented in the previous sections. Figure 4.17 (a-b) and Figure 4.18 (a-b) display the percent reductions in base shear and IDR for the 10% and 20% critical damping structure subjected to the LA11 earthquake.

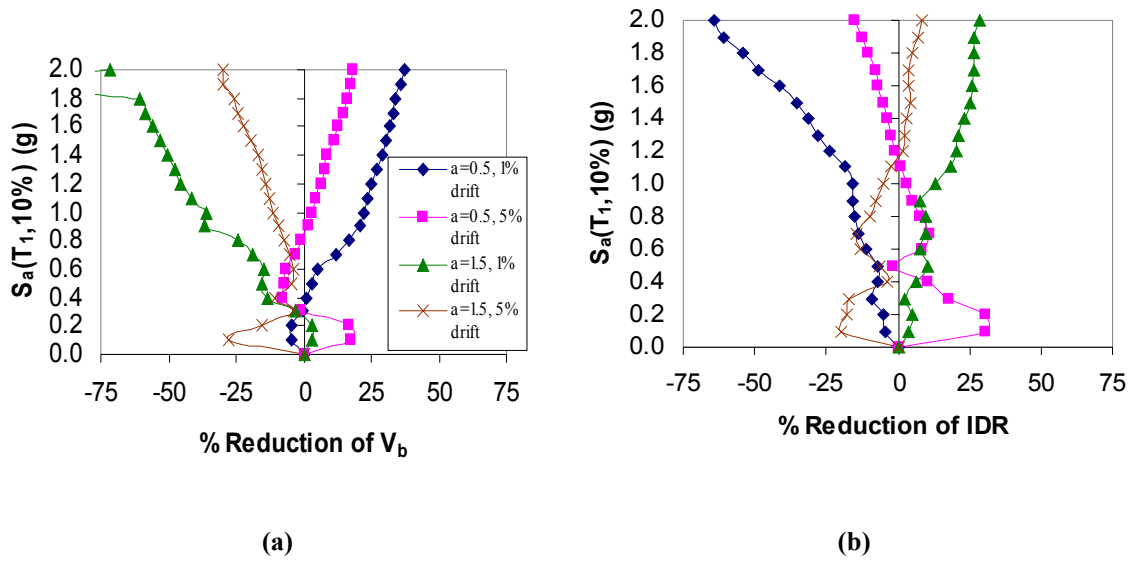


Figure 4.17 (a-b): Percent Reductions of Peak Base Shear and Peak IDR for LA11 w/ 10% Critical Damping

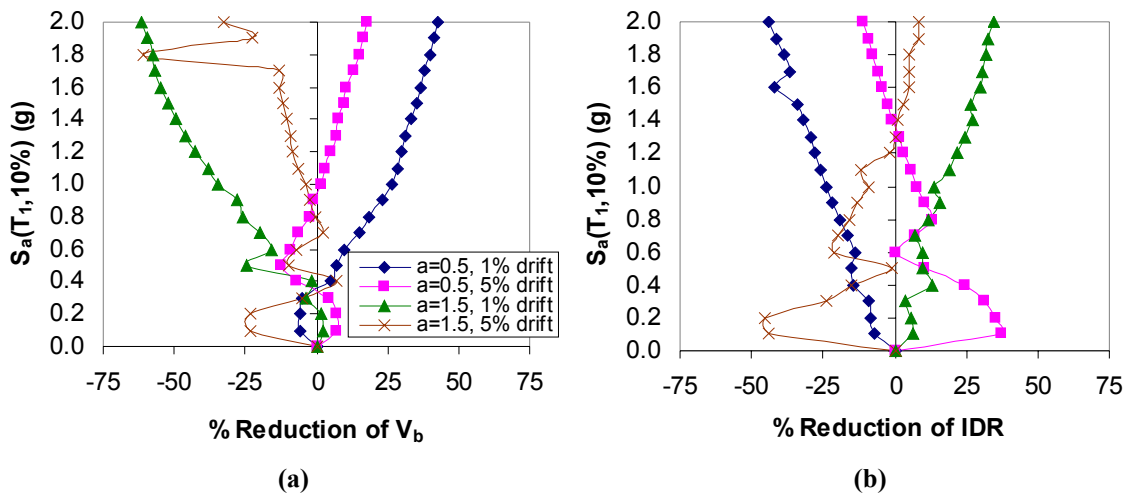


Figure 4.18 (a-b): Percent Reductions of Peak Base Shear and Peak IDR for LA11 w/ 20% Critical Damping

The plots for both 10% and 20% critical damping illustrate the behavior discussed in the two previous sections. The plots displayed here are for one of the LA ground motions, but the behavior is similar for all of the ground motions, including the NF ground motions. Percent reduction plots for each ground motion are displayed in Appendix 2.

Nonlinear damping with $\alpha < 1$ reduces base shear and increases IDR, and when $\alpha > 1$ the opposite occurs. An interesting behavior to note in Figure 4.17 (a-b) and Figure 4.18 (a-b) is the performance of the systems at lower earthquake intensities. Near the yield intensity, some of the curves for the different α values flip from positive values to negative, or vice versa. The intensity at which the switch occurs is about the same for the two different types of nonlinear damper calibrated at the same drift. Furthermore, the switch occurs at a higher intensity when the nonlinear damper is calibrated for 5% drift.

The reason that there is this switch can be explained by looking at the force-velocity relationships for the linear and nonlinear dampers. Figure 4.19 displays the force-velocity curves for the three different values of α (0.5, 1.0, and 1.5) with the nonlinear dampers calibrated to the linear damper at two different levels of drift. The points at which the percent reduction curves cross the y-axis will correspond to the points where the force-velocity curves intersect. At this intersection point, the behavior of the nonlinear damper will change depending on its value of α . For example, when $\alpha = 0.5$, before the intersection, the damper produces more force than $\alpha = 1.0$ at a given velocity. However, after the intersection $\alpha = 0.5$ produces less force than $\alpha = 1.0$ at any given velocity. The effect of the force-velocity relationship of the damper on the response is also the reason that the point where the switch occurs is at a higher intensity when the nonlinear dampers are calibrated for 5% drift.

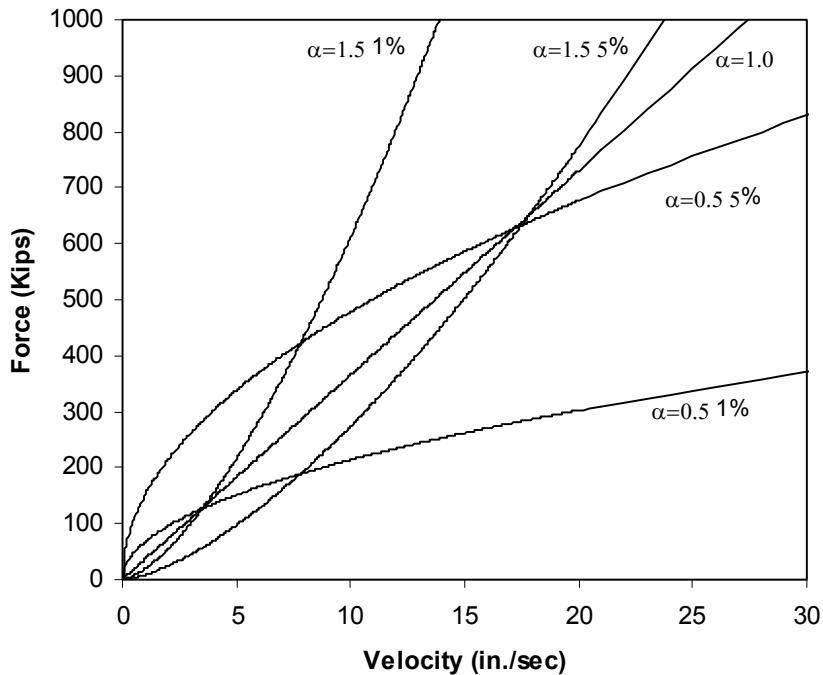


Figure 4.19: Force-Velocity Relationship for Dampers with Different Calibration Constants

This observation demonstrates that the method used to calibrate the nonlinear dampers will have a significant effect on the results of the analysis. The behavior of a system with nonlinear dampers will vary according to the level of drift used in the calibration. The earthquake intensity that produces that level of drift in the structure will also be the intensity where the behavior will change as reflected in the plots.

A final note about the percent reduction plots is that differences between the different damping types are not affected by changes in critical damping. It can be observed in Figure 4.17 (a-b) and Figure 4.18 (a-b) that the values of percent reduction are similar for the 10% and 20% critical damping ratio. This is expected because the structure with nonlinear dampers at 10% critical damping is compared to a structure with linear dampers at 10% critical damping and the same applies for the 20% critical damped case. Therefore, as the amount of critical damping increases, the percentage difference between the nonlinear and linear damping systems does not increase or decrease.

4.3.4 Discussion of Individual IDA Curve Behavior

The following discusses a few different IDA curve behaviors that have been displayed in Figure 4.13-Figure 4.16. A good example of structural softening is illustrated in Figure 4.16 (a). The slope of the curve for $\alpha=0.5$, calibrated for 1% drift, decreases significantly after yield until it is almost zero. This most likely means that the building with these dampers is the most vulnerable to these earthquakes and thus responds very poorly to them. The dramatic increase in IDR with increase in intensity points to the onset of dynamic instability.

A different type of softening is displayed in Figure 4.13 (a) with the curve for $\alpha=1.5$ calibrated for 5% drift. As the curve increases in intensity from $S_a(T_1,10\%)=1.8$ to 1.9 g, the demand for base shear increases significantly. This is most likely the result of a crucial member yielding at the lower intensity and not yielding at the higher intensity. This suggests that the structural behavior is very dependent on the mechanisms that form when the yielding sequence change. The intensity at which this behavior occurs is rather high, so it does not cause much concern; however, the occurrence of an extreme softening near the design spectral acceleration would hint that the structural design was insufficient.

Figure 4.15 (b) and Figure 4.16 (b) provide good displays of structural hardening in the curves for $\alpha=1.5$ calibrated for 1% drift. A possible cause behind this behavior is that at higher intensities the structure undergoes less overall yielding and therefore is better suited to resist the increasing forces that result from the increasing earthquake intensities.

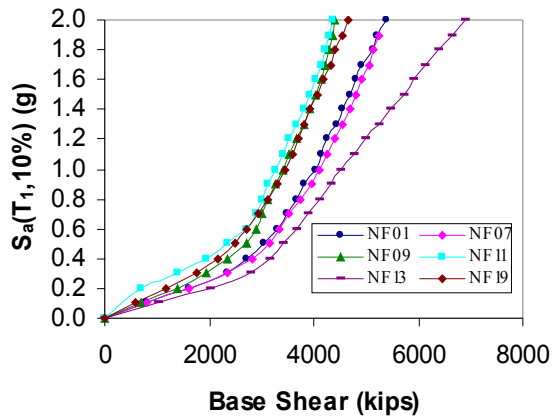
Another interesting behavior, which is shown in Figure 4.16 (b), is a weaving behavior. The slope of the response of the structure associated with $\alpha=1.5$ calibrated at 5% fluctuates between increasing and decreasing values for a range of higher earthquake intensities. This seems abnormal, but one possible explanation is that as the intensity

increases, one peak of a ground motion cycle produces the maximum response, but after a certain point a peak of another cycle that precedes the dominant one becomes strong enough to produce a different yielding sequence. When different component yield first they create a mechanism that helps the rest of the building behave better, and therefore the response is decreased. This happens the most for $\alpha=1.5$ and is observed in both base shear and IDR plots. Researchers in other studies have observed the weaving behavior along with the softening and hardening behavior discussed above. Vamvatsikos and Cornell (2001), in their analysis of the IDA procedure, list all of these behaviors as responses commonly observed when using the IDA approach.

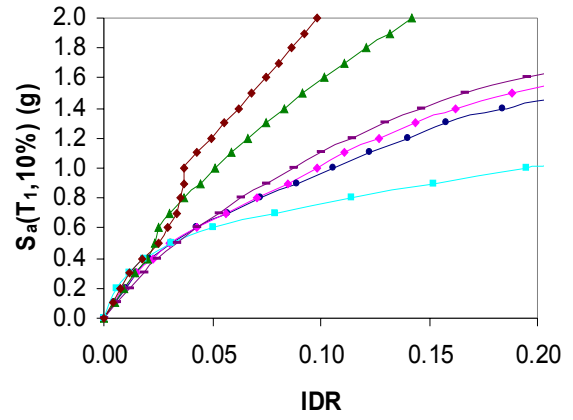
4.4 Multi-Record IDA Curves

An objective of this study is to determine if a certain damper type can reduce the amount of dispersion that occurs in the multi-record IDA plots. These plots display the response of the LA 9-story structure with a certain type of damper calibrated at a specific drift subjected either to the LA or NF ground motions. The dispersion that is experienced in these plots reflect an uncertainty of the behavior of the structure. Ideally, to reduce the uncertainty caused by the dispersion, one would like the lower bound curve to become more like the upper bound curve.

The peak base shear and IDR plots displayed in Figure 4.20 (a-b)-Figure 4.22 (a-b) are multi-record IDA curves for the 20% damped structure with $\alpha=0.5$ at 1% drift, $\alpha=1.0$, and $\alpha=1.5$ at 1% drift respectively. In these plots the structure is subjected to the six NF ground motions. IDA plots for the 10% damped structure subjected to the LA and NF ground motions and the 20% damped structure subjected to the LA and NF ground motions can be found in Appendix B.

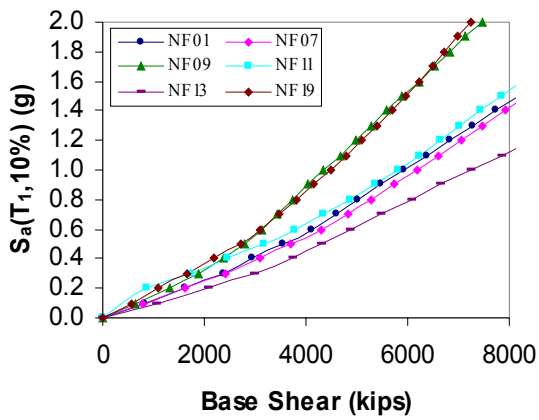


(a)

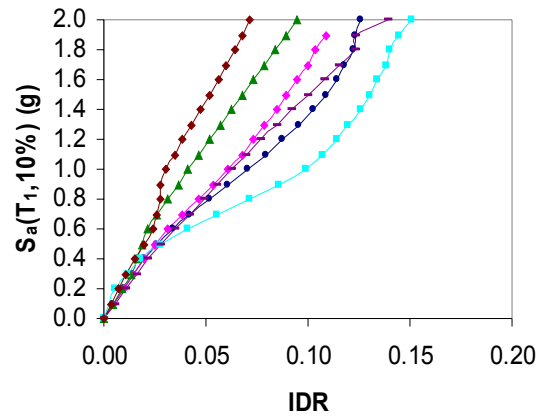


(b)

Figure 4.20 (a-b): Multi-Record IDA Curves for $\alpha=0.5$ at 1% drift 20% damped with NF Ground Motions



(a)



(b)

Figure 4.21(a-b): Multi-Record IDA Curves for $\alpha=1.0$ 20% damped with NF Ground Motions

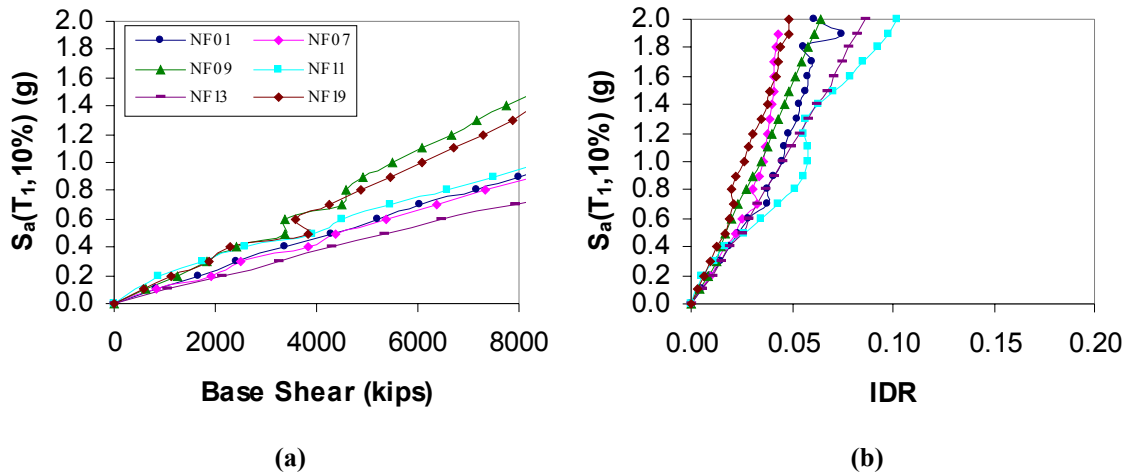


Figure 4.22 (a-b): Multi-Record IDA Curves for $\alpha=1.5$ at 1% drift 20% damped with NF Ground Motions

Figure 4.20 (a-b)-Figure 4.22 (a-b) show that the structure using dampers with $\alpha=1.5$ at 1% drift experiences the least amount of dispersion in IDR results. Conversely, the structure using dampers with $\alpha=0.5$ at 1% has the most amount of dispersion in the drift IDA plots. From these plots it can also be seen that the amount of dispersion between the peak base shear IDA plots increases as the dispersion in the drift plots decreases.

Thus far all of the observations have been somewhat qualitative; therefore standard deviation IDA plots have been created to produce more quantitative observations. The standard deviation of the responses produced by the different earthquakes at each intensity level was calculated for each structure with a different type of damping. The standard deviation will increase as the amount of dispersion increases. When the standard deviation IDA curves for the different types of damping are displayed together, the curve that has the steepest slope will correspond to the system that is best at reducing dispersion.

Figure 4.23 (a-b) displays the standard deviation IDA curves for the 20% critically damped structure with the five different types of damping subjected to the NF ground motions. The behavior displayed in Figure 4.23 is representative for both the 10% and

20% critically damped structure subjected to the NF and LA ground motions. These plots confirm the observation that the structure with $\alpha=1.5$ at 1% has the least amount of dispersion in the IDR results, while $\alpha=0.5$ at 1% has the most amount of dispersion. The base shear standard deviation IDA plots display an opposite behavior. The structure with $\alpha=1.5$ at 1% drift has the most dispersion in the results, while $\alpha=0.5$ at 1% drift shows the least.

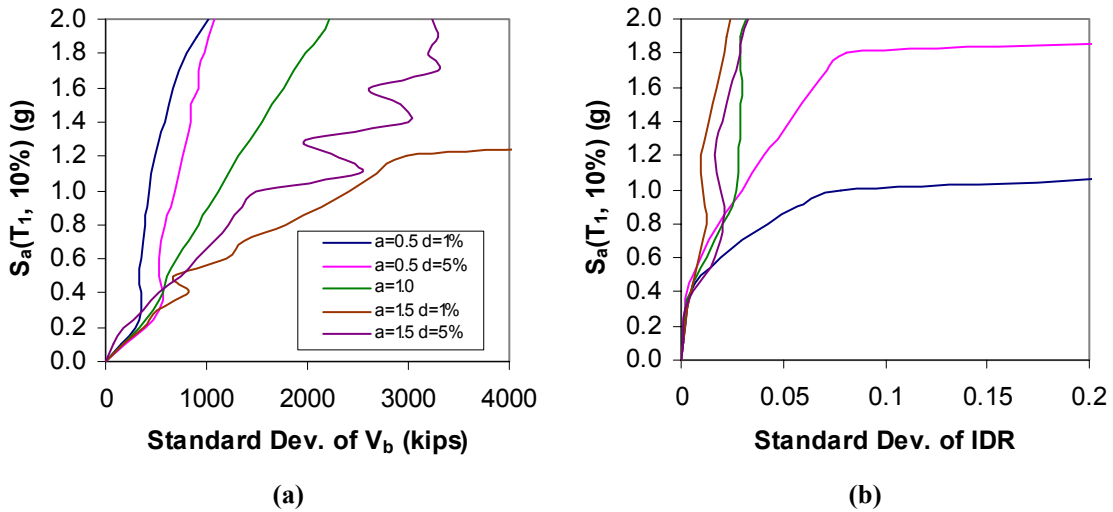


Figure 4.23 (a-b): Standard Deviation IDA Curves of 20% Damped Structure for NF Ground Motions

Figure 4.23 (b) shows that as the intensity increases past 1.0 g and then past 1.8 g the standard deviations for $\alpha=0.5$ at 1% drift and 5% drift increase drastically. This sudden, large increase can be contributed to the structure with these types of damping experiencing severe softening for some of the NF earthquakes, but not all of them. The effect of this on the standard deviation IDA curves may skew the conclusion that can be drawn from the plots. Therefore, IDA plots that focus on the responses at lower intensity are displayed in Figure 4.24 (a-b)

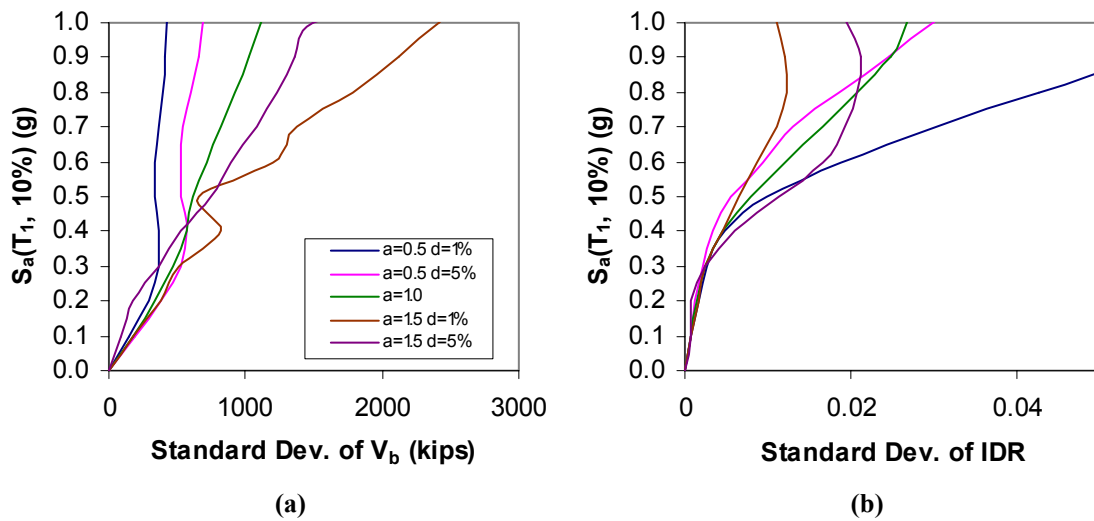


Figure 4.24 (a-b): Close-Up of Standard Deviation IDA Curves of 20% Damped Structure for NF Ground Motions

Figure 4.24 (a-b) still shows that the standard deviation increases the least for $\alpha=1.5$ at 1% drift and the most for $\alpha=0.5$ at 1% drift. However, it may be more interesting to note that the shapes of the standard deviation curves are different for $\alpha=0.5$ and 1.5. The standard deviation curve of IDR for $\alpha=0.5$ has a softening shape, while the $\alpha=1.5$ curve has a hardening shape. Furthermore, the curves for the dampers calibrated at 1% drift intersect near 0.4 g and the curves for the dampers calibrated at 5% drift intersect near 0.8 g. These shapes are similar to the shapes of the force-velocity relations for the different damper types as shown in Figure 4.19. This suggests that the shape of a damper's force-velocity relationship and the calibration parameter influence the amount of variation in structural response to different earthquakes.

The results discussed in this section address the issue of dispersion in the IDA plot. From these results, it can be concluded that the dispersion in the drift IDA plots are best decreased by using nonlinear dampers with $\alpha=1.5$ at 1% drift. However, this reduction of dispersion in the drift result does come at the cost of an increase in dispersion in the base shear results.

4.5 Damage Index IDA Curves

The Park and Ang Damage Index is one of the other response measures that was selected to assess the performance of the structure with different damping types. This damage index (DI) was calculated for the 10% and 20% critically damped LA 9-story structure using dampers with $\alpha=0.5, 1.0,$ and 1.5 subjected to the LA01, LA10, LA13, NF01, NF07, and NF11 ground motions. For these calculations the nonlinear dampers were only calibrated for 1% drift. As discussed in Chapter 3, the DI is calculated for each inelastic girder hinge in the structure, then a weighted average is used to determine story DI's and the overall structural DI. The plots presented in this section and in Appendix B display the IDA curves for the overall structural DI.

Figure 4.25(a-b) displays the damage IDA curves for the 10% and 20% critically damped structure using dampers with $\alpha=1.5$ subjected to each of the ground motions. This plot illustrates similar structural behavior to that displayed in the drift multi-record IDA plots. The value of DI is similar for all the records before yield, which is around $S_a(T_1,10\%)=0.3$ g; after yield there is dispersion between the DI's for the different motions. It is important to note that the value of DI before yield is zero. This confirms the DI calibration constant that was chosen so that DI equals zero when the structure remains linear elastic.

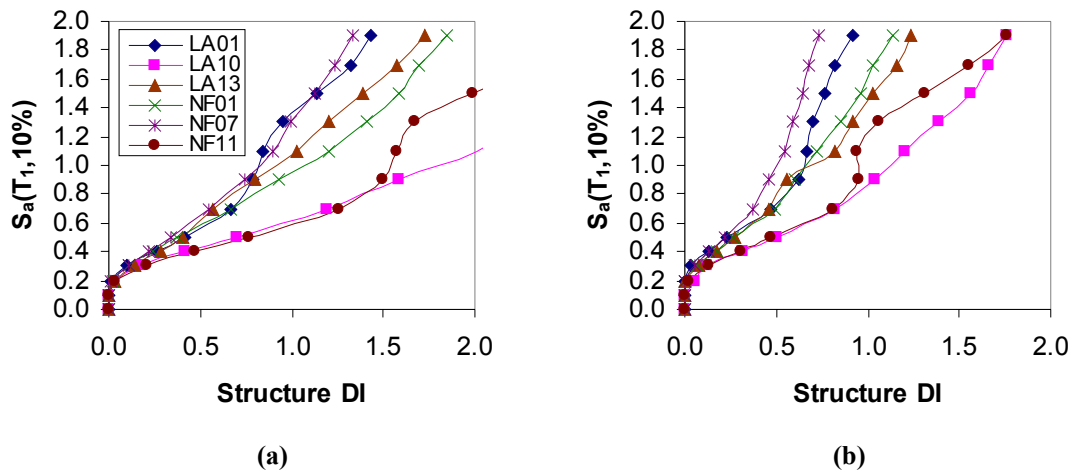


Figure 4.25 (a-b): DI IDA Curves for 10% (a) and 20% (b) Critically Damped Structure w/ $\alpha=1.5$

The previous figure shows that as critical damping ratio increases, the damage in the structure decreases. Figure 4.25 (a-b) is for the structure using dampers with $\alpha=1.5$, but the multi-record DI IDA curves for $\alpha=1.0$ and 0.5 , displayed in Appendix B, illustrate similar behavior. Therefore, regardless of damper type, damage is decreased with increased critical damping ratio.

Figure 4.26 (a-b) is a plot of the IDA curves for the 10% and 20% critically damped structure subjected to the NF07 ground motions. These plots compare the amount of damage produced for the structure when the different types of damping are used. From Figure 4.26 (a-b) it can be concluded that for both the 10% and 20% damped structure the least damage is produced when $\alpha=1.5$, followed by $\alpha=1.0$ and $\alpha=0.5$.

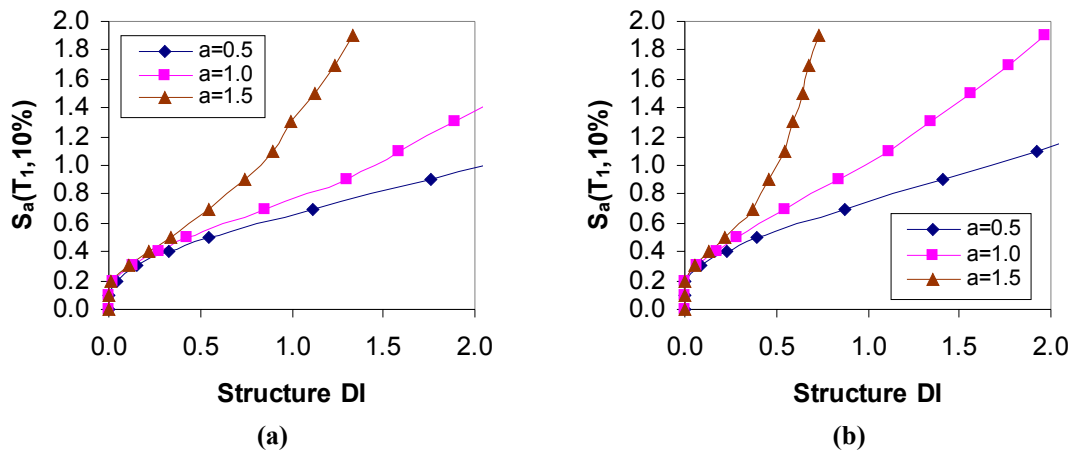


Figure 4.26: DI IDA Curves for 10% (a) and 20% (b) Structure w/ $\alpha=0.5, 1.0, \text{ and } 1.5$ for NF07

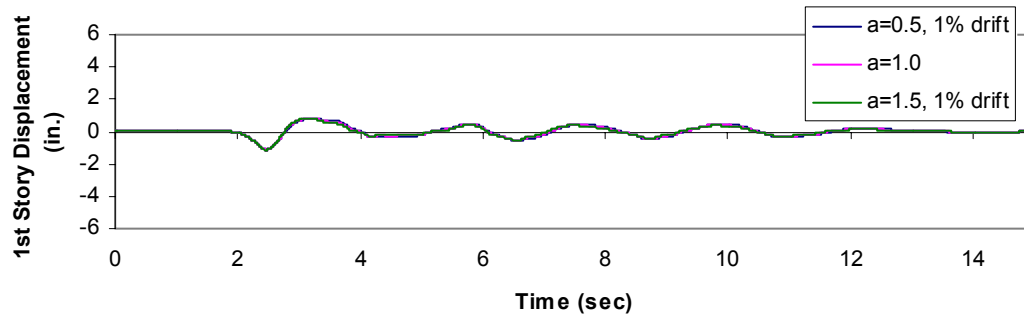
The DI used is calibrated so that a value of unity signifies the collapse of the structure. The IDA curves for NF07 and the IDA curves for the other ground motions, presented in Appendix B, show that the range of intensity when DI equals unity is around 0.6 g to 1.3 g. These intensities are three to six times greater than the design intensity of 0.21 g, indicating that the structure used for the study has a reasonable amount of overstrength. Therefore, the DI with the calibration constant chosen for the study is reasonable for quantifying damage caused in the LA 9-story structure.

4.6 Residual Displacements

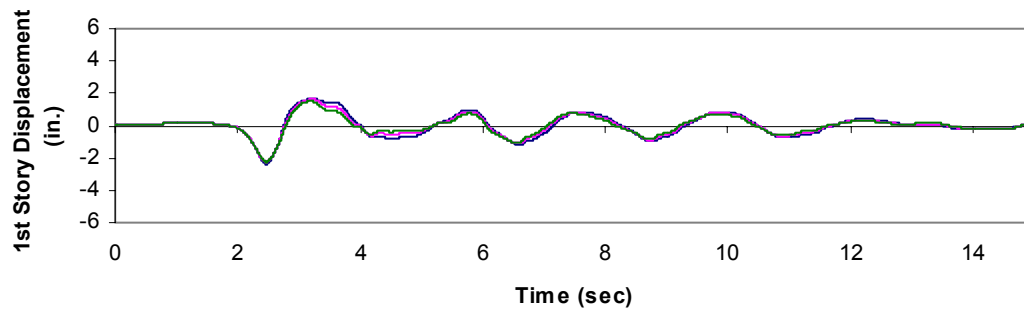
Another objective of this study is to observe if a certain type of damping can reduce residual displacements. Chapter 3 discusses the method used in this study for measuring residual deformations. Residual displacement IDA curves for the structure's first story have been created for the LA 9-story structure, with the 5 different types of damping, subjected to the 12 LA and NF ground motions. A few examples of these IDA plots are displayed and discussed in this section. Furthermore, displacement time history plots of the structure's first story are used to illustrate the effects of the different damper types on residual displacements.

4.6.1 Displacement Time History Plots

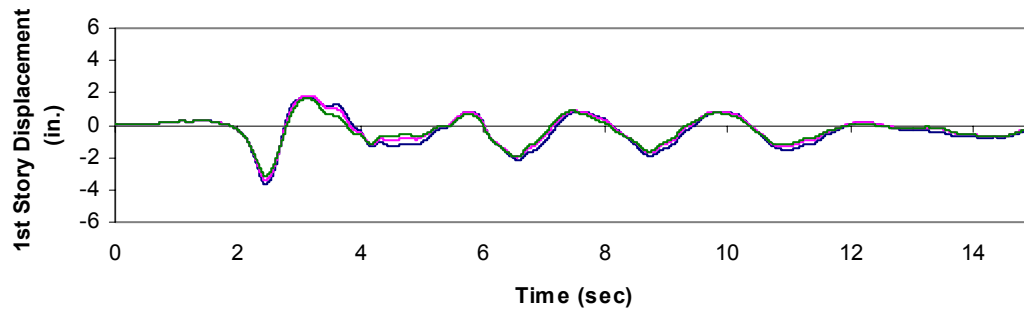
The following time history plots, displayed in Figure 4.27 (a-d) and Figure 4.28 (a-d), provide an example of a structure that undergoes residual displacements. These plots contain three different curves for a 20% critically damped structure using devices with values of α equal to 0.5, 1.0, and 1.5. The nonlinear dampers that are used in this example have been calibrated for 1% drift. Eight different time history plots are displayed for eight different earthquake intensities in order to illustrate the changes in residual displacements with changes in intensity. The earthquake that is used in the time history plots is the NF13 ground motion.



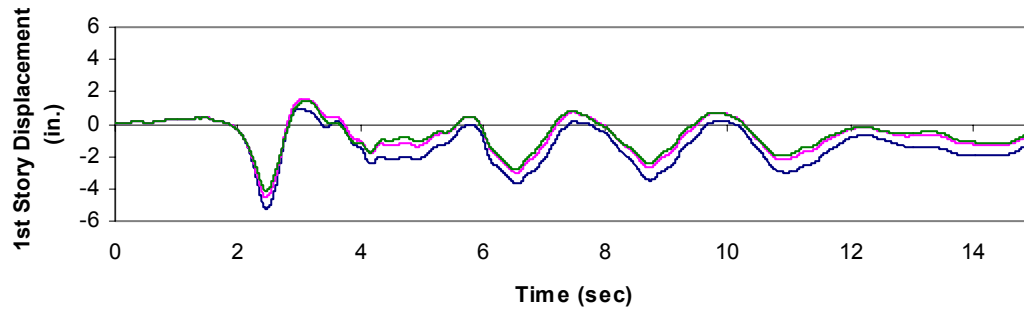
(a)



(b)

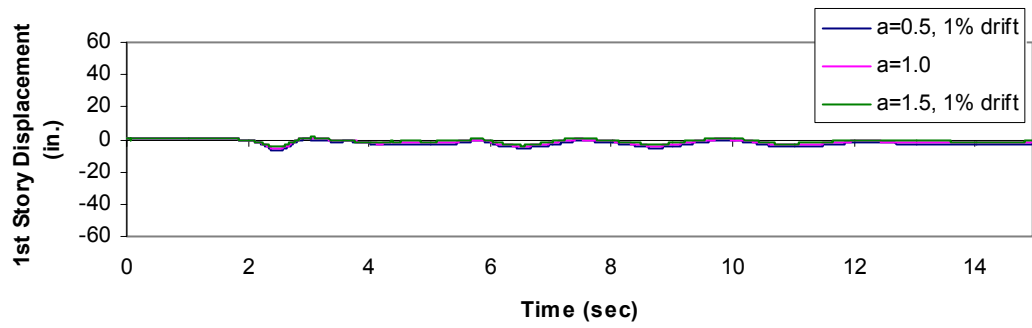


(c)

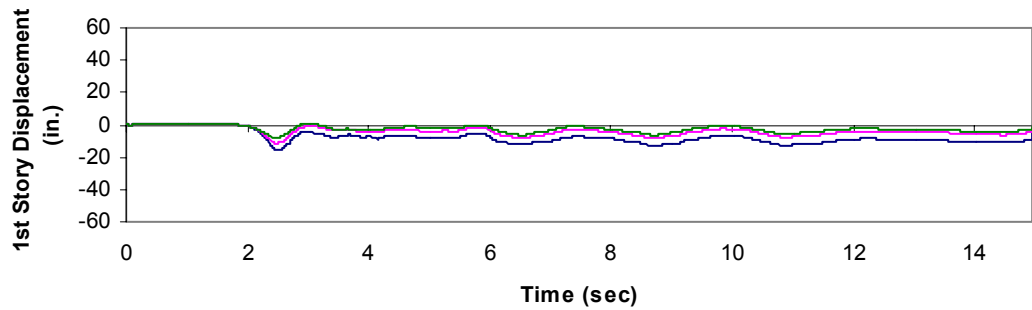


(d)

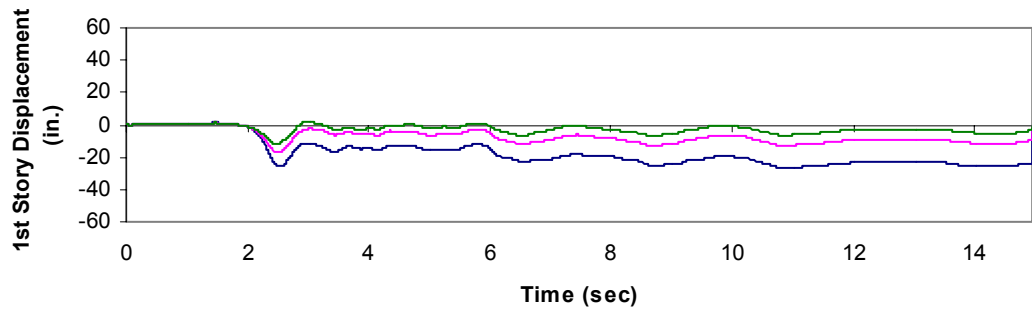
Figure 4.27 (a-d): Displacement Time History Plots for NF13 at $S_a(T_1, 10\%) = 0.1, 0.2, 0.3, \& 0.4$ g



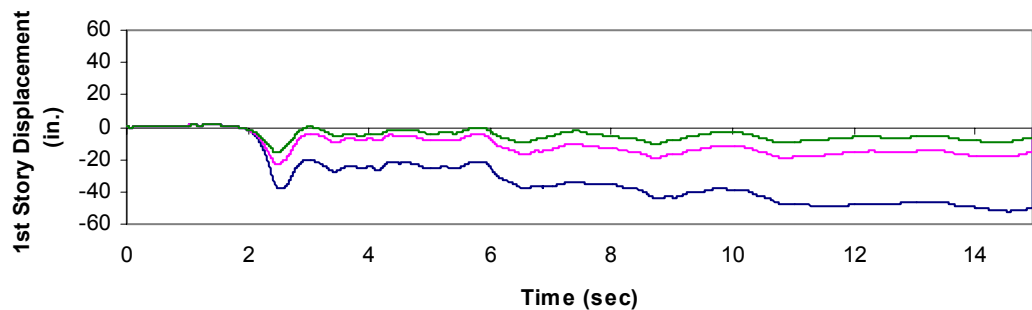
(a)



(b)



(c)



(d)

Figure 4.28 (a-d): Displacement Time History Plots for NF13 at $S_a(T_1, 10\%) = 0.5, 0.9, 1.3, \& 1.7$ g

Figure 4.27 (a-d) and Figure 4.28 (a-d) illustrate that the least amount of residual displacement in the first story of the structures occurs when dampers with $\alpha=1.5$, calibrated at 1% drift, are used. The next best response is when linear dampers are used, followed by dampers with $\alpha=0.5$ calibrated at 1% drift.

4.6.2 Residual Displacement IDA Plots

Residual displacement IDA curves were created to summarize the effect of different damping types, with 20% critical damping, on residual displacements recorded for the 12 earthquakes used in this study. Figure 4.29 is an IDA plot for the NF01 ground motion, including curves for $\alpha=0.5$, 1.0, and 1.5, with the nonlinear dampers calibrated at 1% and 5% drift. This plot illustrates the behavior that is displayed in the time history plots discussed in the previous section. The best response is for $\alpha=1.5$ at 1% drift, followed respectively by $\alpha=1.5$ at 5%, $\alpha=1.0$, $\alpha=0.5$ at 5%, and $\alpha=0.5$ at 1%.

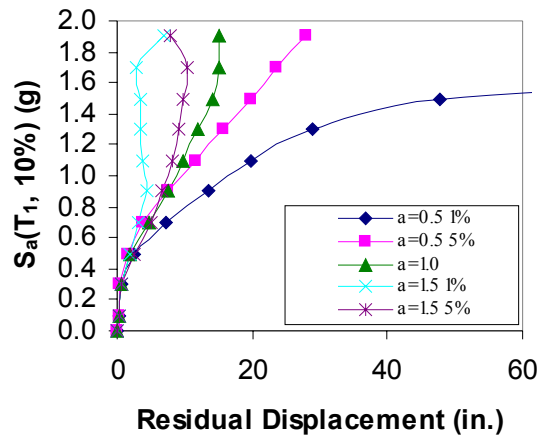


Figure 4.29: Residual Displacement IDA of 20% Critically Damped Structure for NF01

Figure 4.30 displays the response shown in the previous figure for intensities less than and equal to unity. The plot at the lower intensities displays the same general behavior as before; however, it also illustrates the different shapes of the curves for the different damper types. As seen earlier with the standard deviation IDA curves, the residual displacement IDA curve for a certain damper type takes on a shape similar to the

damper's force-velocity relationship. Therefore, the ability of a damper to reduce residual displacements in a structure is dependent on its force-velocity relationship and its calibration parameter.

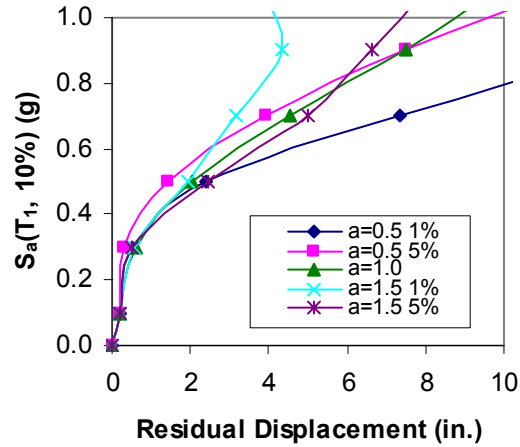


Figure 4.30: Close-Up of Residual Displacement IDA of 20% Critically Damped Structure for NF01

The structural behavior exhibited in Figure 4.29 and Figure 4.30, where there is a relationship between damper type and residual displacement reduction, is not the only behavior that was observed in this study. Figure 4.31 is a residual displacement IDA plot for the LA17 ground motions, including all the different types of damping.

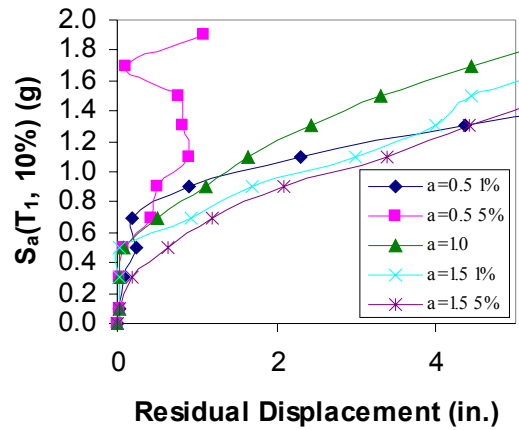


Figure 4.31: Residual Displacement IDA of 20% Critically Damped Structure for LA17

This figure shows that the best response is for $\alpha=0.5$ at 5% drift followed respectively by $\alpha=1.0$, $\alpha=0.5$ at 1% drift, $\alpha=1.5$ at 1% drift, and $\alpha=1.5$ at 5% drift. From this observation, it seems reasonable to conclude that there is no clear relationship between type of damping and reduction of residual displacements. However, it can also be seen in Figure 4.29 and Figure 4.31 that there is a significant difference in the size of the residual displacements for the two earthquakes. Other IDA curves in Appendix 2 also show that the earthquakes that do not produce any relationship between damper type and residual displacement tend not to produce large values of residual displacement.

Table 4.1 lists the residual displacements for a structure with linear dampers subjected to an earthquake with an intensity of 0.9 and 1.1 g. In this table the residual displacements have been separated into two categories: one is for ground motions where the aforementioned relationship between damper type and residual displacements exists, and the other is where there is no relationship.

Table 4.1: Residual Displacements for Structure with Linear Dampers

Residual Displacements (in.)							
$S_a(T_1, 10\%)=0.9\text{ g}$				$S_a(T_1, 10\%)=1.1\text{ g}$			
Ground Motions with Relationship		Ground Motions without Relationship		Ground Motions with Relationship		Ground Motions without Relationship	
LA01	6.92	LA07	3.01	LA01	8.02	LA07	4.26
LA10	8.52	LA11	1.79	LA10	9.79	LA11	2.72
LA13	6.32	LA17	1.11	LA13	7.95	LA17	1.63
NF01	7.50	NF09	0.35	NF01	9.89	NF09	0.74
NF07	5.74	NF19	1.16	NF07	7.70	NF19	0.65
NF11	15.06			NF11	17.39		
NF13	5.28			NF13	7.55		
Average	7.91	Average	1.48	Average	9.76	Average	2.00

The table shows that at two different intensities the ground motions with a relationship have larger values of residual displacements than the ground motions with no relationship. Not only is the average higher, but also any ground motion in the first category has a larger value than any in the second category.

A reason for this behavior may, once again, be related to the force-velocity relationships of the different types of dampers, as shown in Figure 3.16. As discussed earlier, each nonlinear damper force-velocity curve will intersect the linear curve at the specified level of velocity. At these intersection points, or at points where two nonlinear dampers intersect, the two dampers will produce the same amount of force for the same velocity. Before the intersection a nonlinear damper, with a value of $\alpha=0.5$, will experience a higher force at a given velocity than the linear damper. After the intersection the opposite will be true. The differences between force-velocity relationship for two different damper types are most noticeable in the residual displacement IDA curves when the residual displacements are small. An example of this can be seen in a residual displacement IDA plot for LA11 displayed in Figure 4.32.

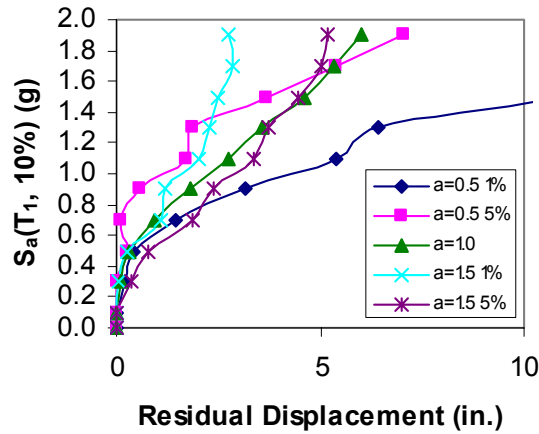


Figure 4.32: Residual Displacement IDA of 20% Critically Damped Structure for LA11

In Table 4.1, it is listed that there is no relationship between damping type and residual displacements when the structure is subjected to the LA11 ground motions. This was determined by the uncharacteristic response with $\alpha=0.5$ calibrated at 5% drift. Figure 4.32 illustrates that this curve indicates a much better response than the previously defined relationship justifies. However, if the small value of residual displacement is considered, it looks as if the nonlinear damper with $\alpha=0.5$ at 5% drift only reaches 5% drift at a high level of intensity. At 5% drift the curve looks as if it will fall in line with the expected relationship. Therefore, if this earthquake produced a more severe response, the relationship between damper type and reductions of residual displacements would exist.

These findings suggest the importance in considering the method used to calibrate dampers when analyzing the results of a comparison. However, since the relationship between damper type and residual displacements only varies when the residual displacements are small, it is less of a concern because small residual displacements are a less significant threat to the structure. Therefore, a reasonable conclusion is that a

structure using dampers with $\alpha=1.5$ at 1% is the best system to reduce residual displacements.

An interesting deviation from the relationship is seen in the structure subjected to the LA01 ground motion. The IDA plot for LA01 is listed under the first category in Table 4.1 even though the curve for $\alpha=0.5$ at 1% drift does not behave exactly as expected. Figure 4.33 displays that as the intensity increases past 0.9 g the residual displacements in the system with $\alpha=0.5$ at 1% drift decrease.

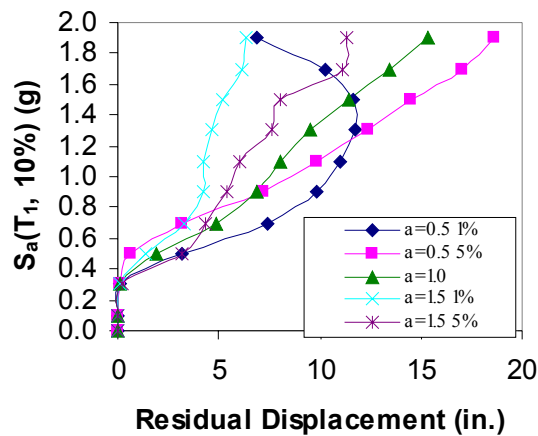
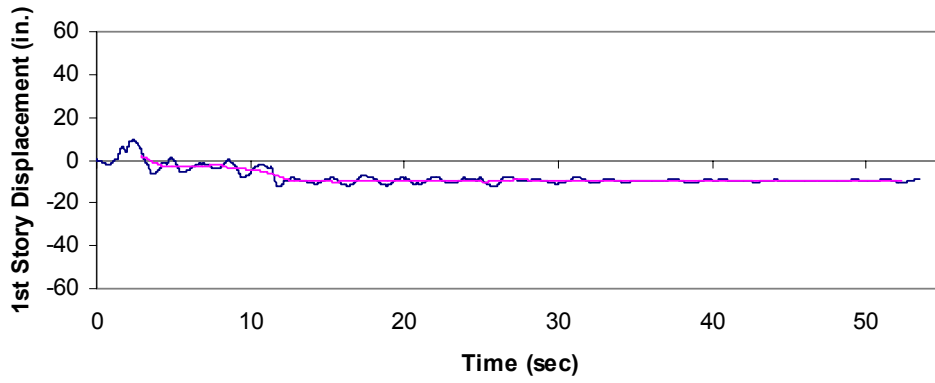
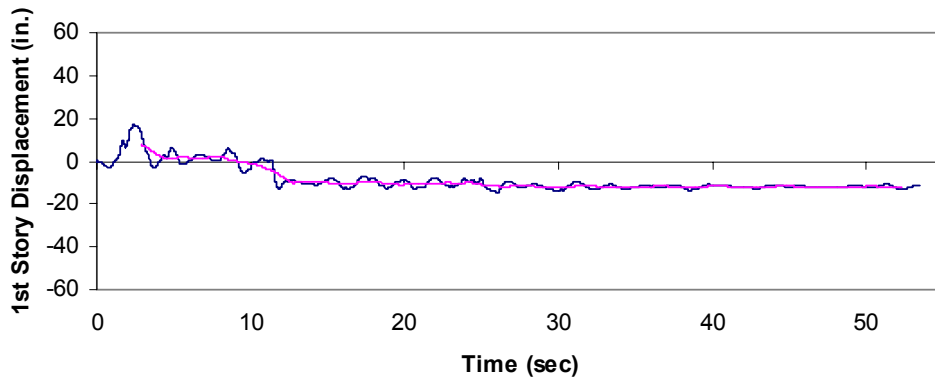


Figure 4.33: Residual Displacement IDA of 20% Critically Damped Structure for LA01

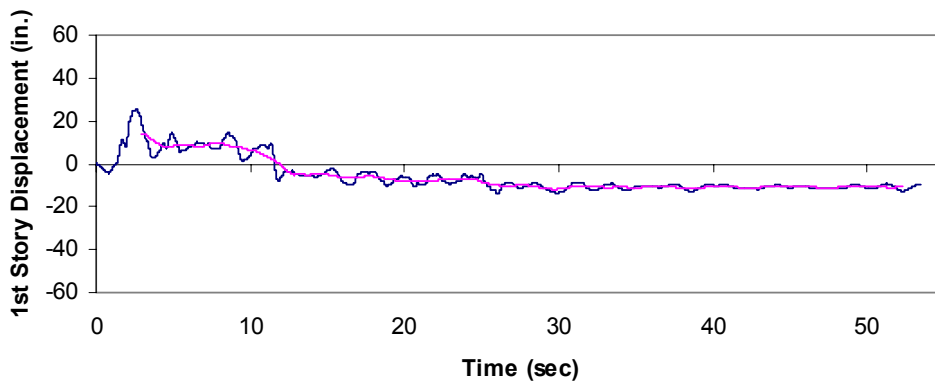
This abnormal behavior can be explained by comparing time history plots of the structure for $\alpha=0.5$ at 1% and 5% drift. Figure 4.34 (a-c) and Figure 4.35 (a-c) each display the time history plots for the two nonlinear dampers at intensities of 0.9, 1.3, and 1.7 g, respectively. The red line in the plots is the baseline residual displacement that is calculated using the method described in Section 3.3.4



(a)

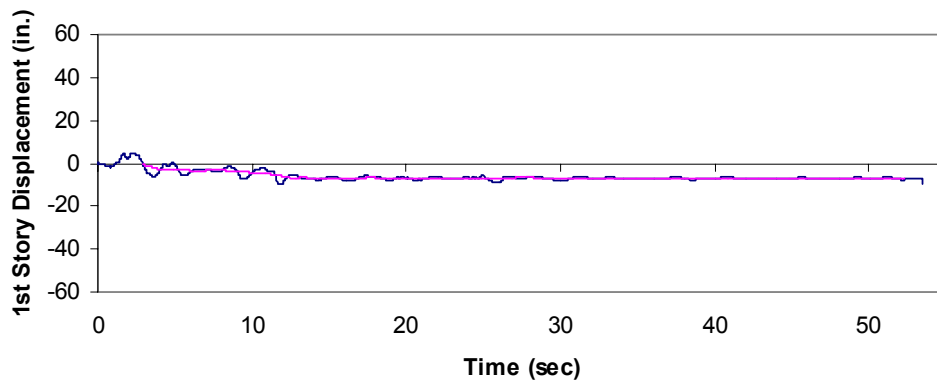


(b)

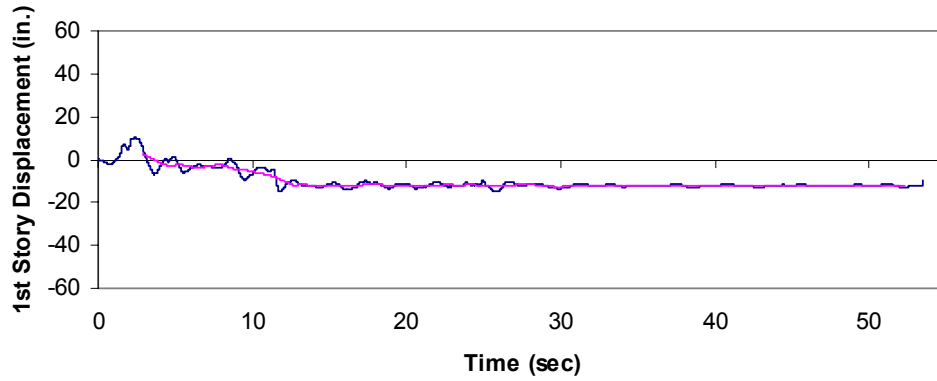


(c)

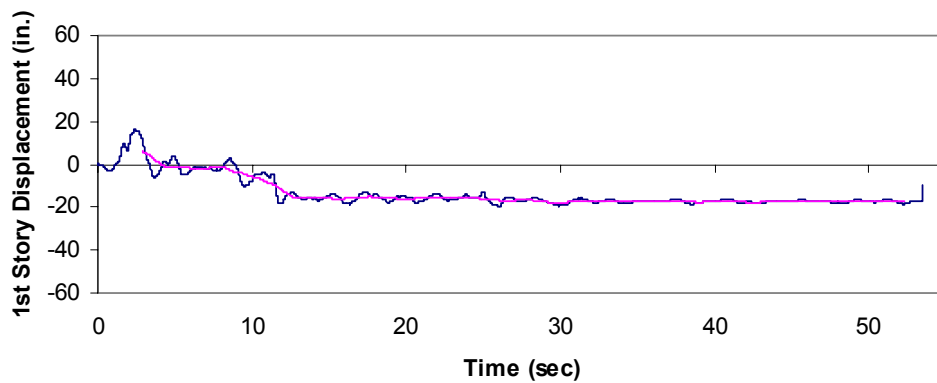
Figure 4.34 (a-c): Displacement Time History Plots $\alpha=0.5$ at 1% Drift 20% Critically Damped for LA01 at 0.9, 1.3, and 1.7 g



(a)



(b)



(c)

Figure 4.35 (a-c): Displacement Time History Plots $\alpha=0.5$ at 5% Drift 20% Critically damped for LA01 at 0.9, 1.3, and 1.7 g

Figure 4.34 (a-c) illustrates that as the intensity increases from 0.9 to 1.7 g, the structure with dampers calibrated at 1% drift initially has a positive residual displacement before shifting to the negative side. The response is different for the structure with dampers calibrated at 5% drift, which is displayed in Figure 4.35 (a-c). These plots show the residual displacements to be in only one direction. The initial positive response in the structure with dampers at 1% seems to be responsible for the lower overall amount of residual displacement at the end of the history.

There may be several different reasons for the change in direction of the response; one possibility could be related to the relationship between sequence of peak acceleration cycles and sequence of yielding members. Regardless, the variation in the direction of the deformation appears to be the reason that the overall residual displacements decreased with increasing earthquake intensity. Therefore, it is assumed that the behavior exhibited in the LA01 residual displacement IDA plot, displayed in Figure 4.33, is similar to the behavior discussed at the beginning of this section. From this it can be concluded that when using dampers in structures subjected to ground motions that produce residual displacements the effectiveness of damper type can be listed in the following order from best to worst: $\alpha=1.5$ calibrated at 1% drift, $\alpha=1.5$ calibrated at 5% drift, $\alpha=1.0$, $\alpha=0.5$ calibrated at 5% drift, and $\alpha=0.5$ calibrated at 1% drift.

Prior to the investigation it was expected that the NF ground motions would produce the largest residual displacements. However, Table 4.1 shows that there is no direct connection between the NF ground motions and large residual displacements.

4.7 Relating Dispersion to Residual Displacements

An objective of the study was to observe whether residual displacements are the cause of the dispersion displayed in the IDA plots. The results show that dampers with $\alpha=1.5$ are the best for reducing dispersion and residual displacements, but there is nothing that clearly relates dispersion and residual displacements. Table 4.2 lists the standard

deviation of the drift and the average residual displacement for the structure using dampers with $\alpha=0.5$ and 1.5 at 1% drift subjected to NF and LA ground motions. The values listed show that IDR is larger when the residual displacement is larger. Figure 4.36, which uses the values displayed in Table 4.2, is a plot of the standard deviation of IDR versus the average residual displacement for both the LA and NF and $\alpha=0.5$ and $\alpha=1.5$. Included in this plot is a trend line that illustrates the relationship between residual displacement and standard deviation of IDR. This confirms original expectations that residual displacements are a significant cause of dispersion in the IDA plots.

Table 4.2: Standard Deviation of IDR and Average of the Residual Displacements for LA and NF Ground Motions when Dampers with $\alpha=0.5$ and 1.5 are used

$S_a(T_1, 10\%)$ (g)	$\alpha=0.5$				$\alpha=1.5$			
	LA		NF		LA		NF	
	Std. IDR	RD Avg. (in.)	Std. IDR	RD Avg. (in.)	Std. IDR	RD Avg. (in.)	Std. IDR	RD Avg. (in.)
0.3	0.0019	0.16	0.0026	0.39	0.0024	0.14	0.0024	0.32
0.7	0.0226	4.60	0.0302	6.79	0.0096	2.04	0.0111	2.43
1.1	0.3223	27.40	0.2695	28.81	0.0119	3.44	0.0099	2.80
1.5	0.2584	25.17	0.2956	40.59	0.0144	4.70	0.0158	2.92
1.9	0.4202	52.82	0.3244	67.61	0.0130	5.46	0.0221	3.38

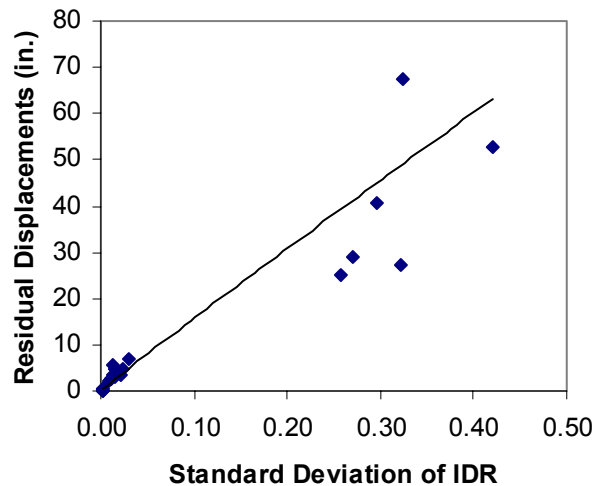


Figure 4.36: Standard Deviation of IDR vs. Residual Displacement

4.8 Dampers with Yielding Braces

Initially, in Chapter 3, the assumption was made that the chevron braces that are used to incorporate the dampers into the structure would not be allowed to yield. This was done because it was felt that it was possible to design the braces for any of the forces they would be subjected to in the study. After some of the analyses were run, it was observed that the brace forces were substantially large, especially with $\alpha=1.5$. Figure 4.37 displays a brace force IDA plot for the 10% critically damped LA 9-story structure with three different types of damper subjected to the NF01 and NF11 ground motions.

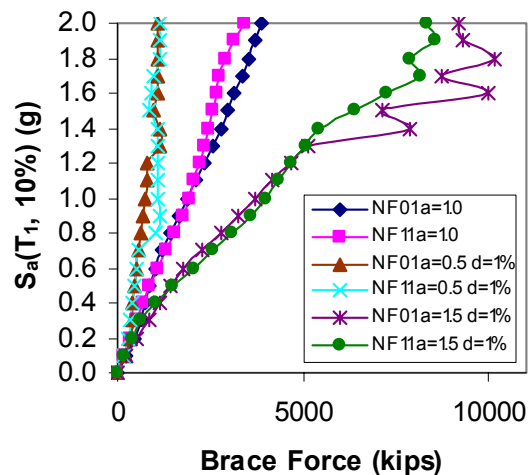


Figure 4.37: Brace Force IDA of 10% Critically Damped Structure for NF01 and NF11

From this IDA plot it can be seen that when $\alpha=1.5$ at 1% drift the brace forces reach about 4000 kips at $S_a(T_1, 10\%)=0.8$ g and 10,000 kips at 2.0 g. These brace forces at the larger intensity are unreasonable for the 10% critically damped structure and will only increase with an increase to 20% critically damped systems. Therefore, further analysis was performed for a structure that used a damping system where the braces were allowed to yield.

The original LA 9-story structure was modified to include the yielding braces by including an inelastic spring in the support that connects the damper to the frame. Figure 4.38 illustrates how the inelastic spring is included into the system through the use of a single-story frame. The inelastic spring is elastic perfectly plastic so that once the forces exceed the yield strength, the braces do not contribute any stiffness. The initial stiffness of the spring was set to a large value, 5,000,000 kips/in., so that the spring was essentially rigid before yield. The design level earthquake in this study has a value of $S_a(T_1,10\%)=0.217$ g, so it was decided that the braces should be designed to resist the maximum force for any of the 12 earthquakes used at an intensity of 0.3 g.

The maximum brace force demand was found to be 2500 kips, and by using static equilibrium the following equation can be found:

$$F_s = 2F_B \cos \theta \quad 4.1$$

where θ is the angle of the brace. The yield strength of the inelastic spring was calculated to be 3200 kips.

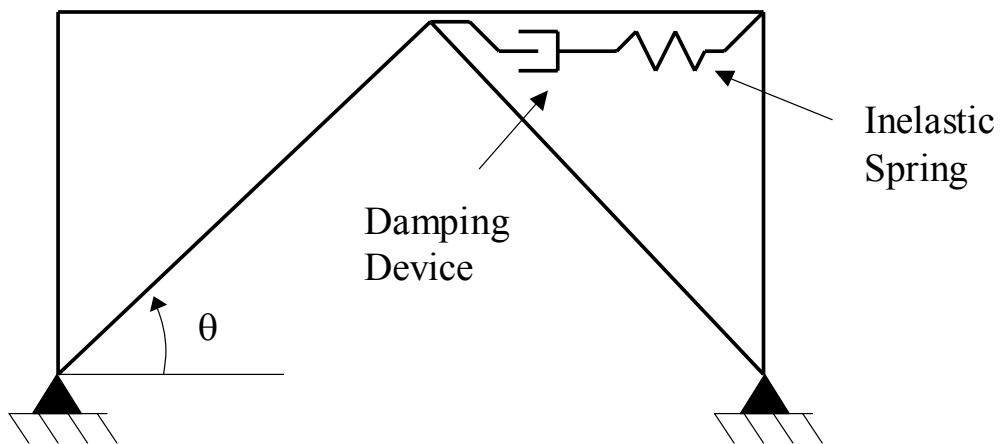


Figure 4.38: Single-Story Damping Frame w/ Inelastic Spring

Previous analysis was repeated now with the yielding braces for the LA01, LA10, NF01, NF07, and NF11 ground motions. These ground motions were selected for this additional analysis because they exhibited the largest reduction in IDR when nonlinear

dampers were used. The analysis was also only repeated for the 20% critically damped structure with $\alpha=0.5$, 1.0, and 1.5 and the nonlinear dampers calibrated at 1% drift. This was done because previous analysis has shown that these are the most extreme cases.

4.8.1 Peak Base Shear and Peak IDR for Structure with Yielding Braces

The effect of the yielding braces was different for the different types of damping. When $\alpha=1.5$ the effect was the greatest, followed by $\alpha=1.0$ and $\alpha=0.5$. Figure 4.39 (a-b) displays the peak base shear and drift IDA plot for the structure with $\alpha=1.5$ subjected to the NF01 ground motion. From these plots it can be seen that the behavior of the two systems is the same for both base shear and IDR until the intensity reaches about 0.5 g. After this point the performance of the system with yielding braces improves with respect to peak base shear. However, at the same time, the response of the system with yielding braces in terms of peak IDR worsens. The behavior displayed in Figure 4.39 (a-b) is similar for all the ground motions, LA and NF, used in this analysis.

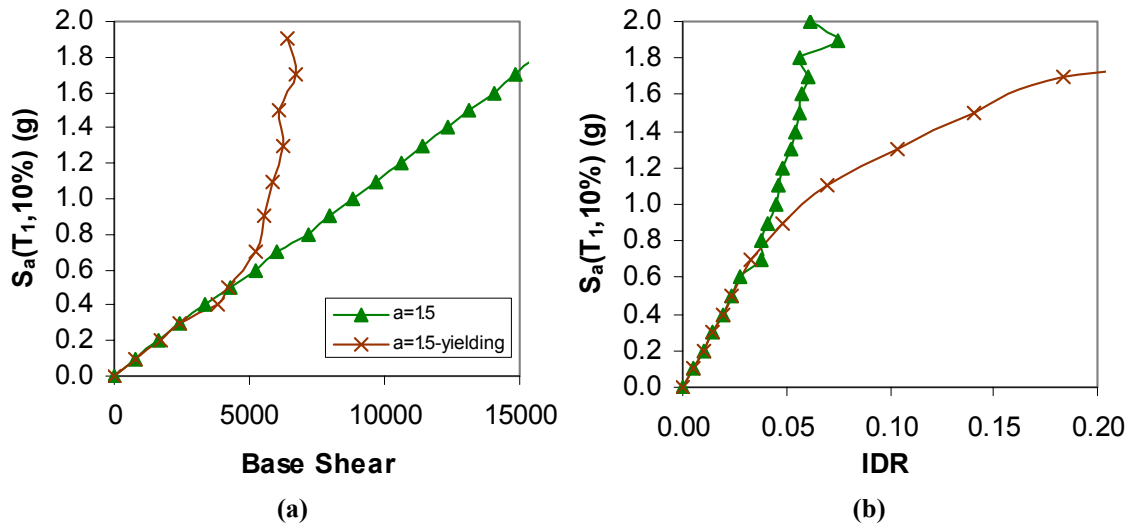


Figure 4.39 (a-b): IDA Plots for $\alpha=1.5$ at 1% Drift 20% Critically Damped NF01

When the yielding braces are included in the structure with linear dampers ($\alpha=1.0$) the behavior changes in the same manner as for $\alpha=1.5$, except the point where the behavior changes occurs at a higher intensity. This is illustrated in Figure 4.40 (a-b), which shows

the peak base shear and IDR IDA plots for the structure with linear dampers subjected to the NF01 ground motion. The changes in these plots occur at an intensity of about 1.1 g.

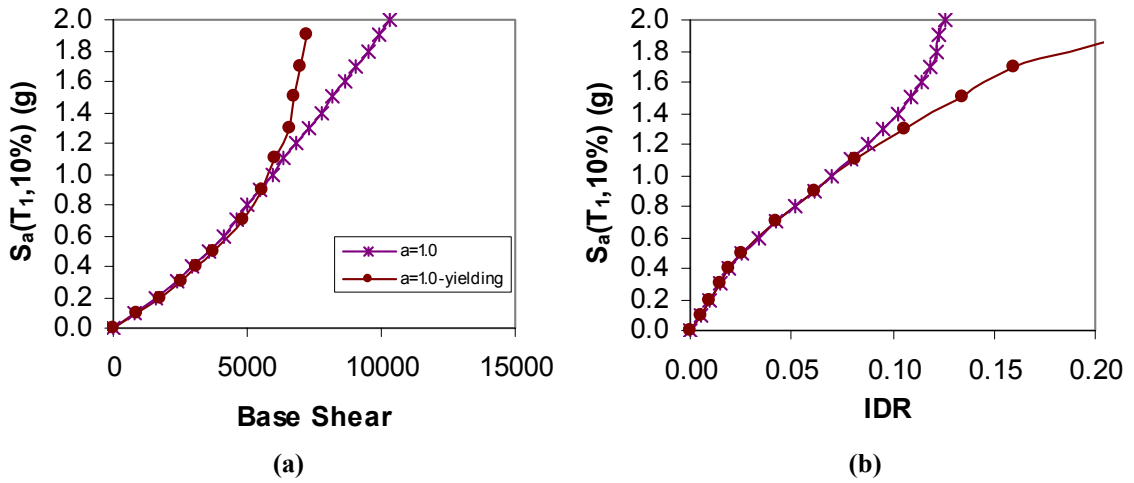


Figure 4.40 (a-b): IDA Plots for $\alpha=1.0$ 20% Critically Damped NF01

The final type of damping that was investigated for a structure including yielding braces was $\alpha=0.5$ at 1% drift. Figure 4.41 (a-b) provides an example of the behavior when this type of damping is used in the structure subjected to the NF01 ground motion. These plots demonstrate that the yielding braces increase the base shear at high levels of intensity, but do not significantly affect the IDR response. The reason that there is no significant change in the IDR is due to the braces remaining elastic for a large range of intensities.

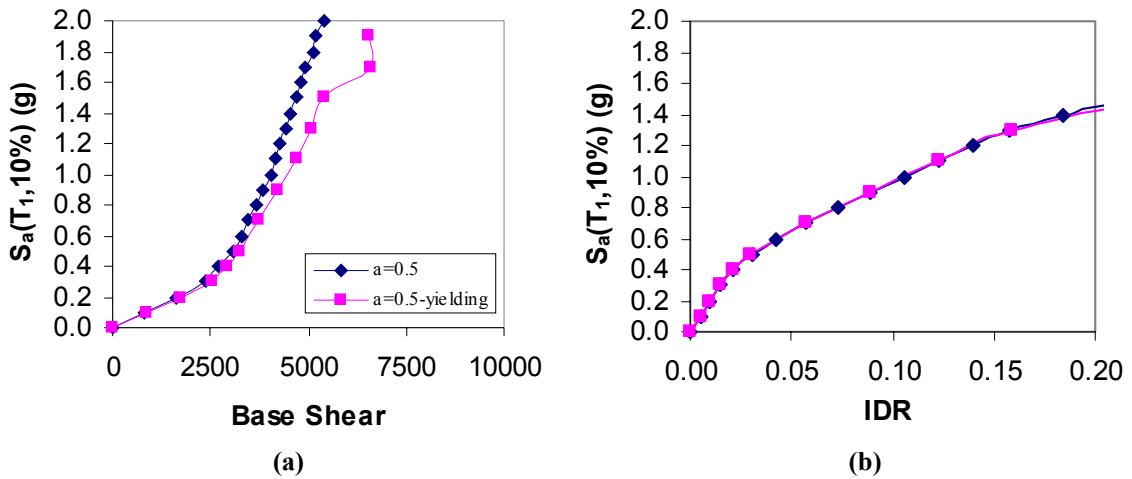


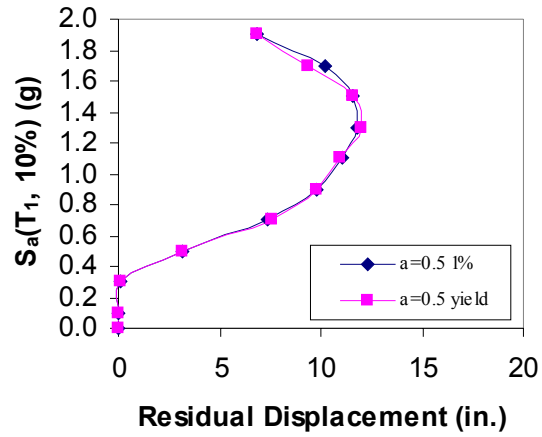
Figure 4.41(a-b): IDA Plots for $\alpha=0.5$ at 1% drift 20% Critically Damped NF01

The behavior of the structure with yielding braces and different types of damping, as displayed in Figure 4.39 (a-b)-Figure 4.41 (a-b), is expected. The more significant change in response occurs when $\alpha=1.5$ at 1% drift, which is reasonable because this type of damping produces the largest peak brace forces. After the earthquake reaches the intensity where the braces yield, the dampers become ineffective and unable to reduce drifts. This ineffectiveness to decrease drift results in the dampers not producing forces that will add to the total base shear, thus the base shear will no longer increase.

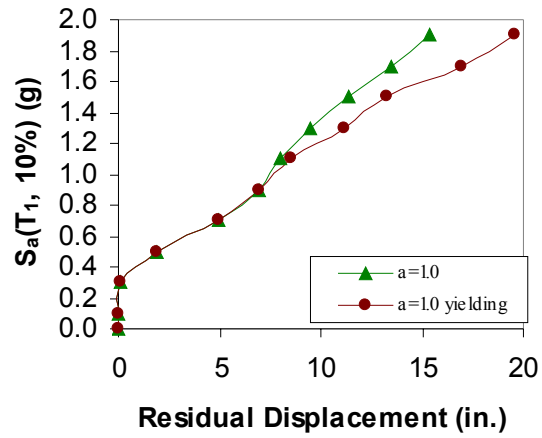
4.8.2 Residual Displacements for Structure with Yielding Braces

The effect of yielding braces on the reduction of residual displacements was also investigated. Earlier analysis found that when dampers with $\alpha=1.5$ were used, the amount of residual displacement experienced by a structure could be reduced. However, as seen previously, the brace forces produced by a damper with $\alpha=1.5$ are significant. Therefore, further analysis was needed to determine whether residual displacements could be reduced when the braces yielded.

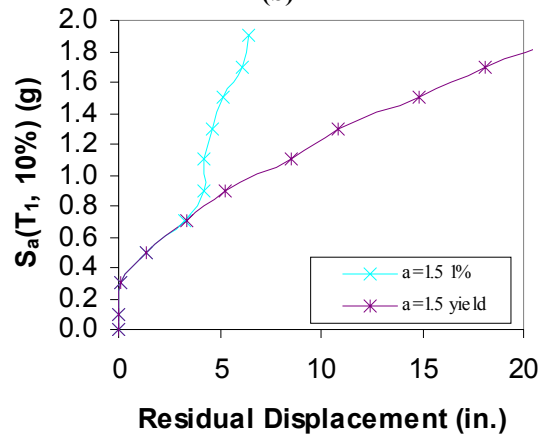
Figure 4.42 (a-c) is an example of the behavior displayed in the residual displacement IDA plots for the structure with $\alpha=0.5$, 1.0 and 1.5, respectively. These plots of the structure subjected to the LA01 ground motion illustrate the behavior that was discussed earlier in section 4.6.1 for drift. When $\alpha=0.5$ at 1% drift, the residual displacement response is the same for the structure with or without yielding braces. The response of the structure with linear dampers is the same with or without yielding braces for intensities that range from 0 to 1.1 g. After that point the residual displacements increase more for the structure with yielding braces. This same behavior occurs for the structure using dampers with $\alpha=1.5$ at 1% drift, but the intensity where the response with and without yielding braces diverges is only 0.7 g.



(a)



(b)



(c)

Figure 4.42 (a-c): Residual Displacement IDA for LA01 $\alpha=0.5, 1.0, \text{ and } 1.5$ 20% Critically Damped

From the IDA plots of residual displacement as well as peak base shear and IDR, it can be concluded that yielding braces can have a significant effect on response based on the brace design. Originally it was assumed that the braces would not yield. If this assumption were an actual representation of real life, then the structure using dampers with $\alpha=1.5$ would be the best for reducing peak IDR and residual displacements. However, it becomes unreasonable if the structure is subjected to ground motions at high intensities.